Journal of Materials Chemistry A

ROYAL SOCIETY OF CHEMISTRY

REVIEW

View Article Online
View Journal | View Issue

Published on 30 September 2020. Downloaded by University of Western Ontario on 1/24/2021 7:05:58 PM.

Check for updates

Cite this: J. Mater. Chem. A, 2020, 8, 21408

Progress in energy-related graphyne-based materials: advanced synthesis, functional mechanisms and applications

Yanmei Gong,†[a] Lihua Shen,†[a] Zhaoming Kang,†[a] Kangfei Liu,†[a] Qixing Du,†[a] Daixin Ye,*[a] Hongbin Zhao,*[a] Xueliang Andy Sun[b] and Jiujun Zhang*[a]

Received 21st June 2020
Accepted 24th September 2020

DOI: 10.1039/d0ta08521a

rsc.li/materials-a

Graphynes (GYs) are the new star carbon isomers with two-dimensional layered in-plane porous structures, which are composed of sp- and sp^2-hybrid carbon atoms. These special features result in their unique topological and electronic structures, high charge mobility and excellent electronic transport properties. All of these advanced properties of GYs make them promising in various applications. In the GY family, graphdiyne (GDY) was the first successfully prepared member, so it attracted the most attention. In this review, the recent progress on the synthetic strategies, functional mechanisms and applications of GDY and other GYs in the fields of energy storage/conversion are summarized, and the challenges hindering their large-scale fabrication toward practical applications are analyzed. Finally, the possible research directions for overcoming the challenges are proposed based on the development trend and perspectives of GYs. It is hoped that this review is helpful for deeply understanding GYs and GY-based materials.

1. Introduction

Carbon materials are probably one of the most useful materials in many areas, including energy sources, manufacturing, and biological medicine. Since the first non-natural carbon allotrope-fullerene was discovered, various carbon materials (as shown in Fig. 1) have been artificially synthesized and attracted great interest from scientific researchers. These carbon materials have extraordinary optical, electronic, thermal, chemical and mechanical properties due to the special electronic structure. For example, as a type of two-dimensional (2D) carbon nanomaterials, graphene is composed of carbon atoms with sp^2-hybrid orbitals and has a hexagonal honeycomb lattice.[1] Because of the internal electronic structure, graphene shows excellent electric, optical, and mechanical properties.[2,3] Now, graphene-based materials could be prepared on a large scale, and many graphene-related products have been used in water and air purification, flexible electronics and wearable areas, industrial surface corrosion resistance, and new energy materials. However, GYs are still in its infancy, and there is still much space for their development.

1.1 Structures of GYs

Graphynes (GYs) are a new type of carbon allotrope that has a sp- and sp^2-hybrid 2D planar network structure formed by binding benzene rings through acetylene bonds, as shown in Fig. 1g. A general name of graph-*n*-yne ($n = 1, 2, 3\ldots$, where n is the number of acetylenic chains) can be given according to the number of acetylenic chains between the adjacent benzene rings contained in a GYs unit. In 1987, Baughman *et al.*[4] theoretically predicted the existence of GYs. For the experimental synthesis of GYs, Li's group[5] first prepared γ-graphdiyne (GDY) using hexaethynylbenzene (HEB) *via* the Glaser–Hay cross-coupling reaction on a copper surface. Li *et al.*[6] synthesized a thin film β-graphdiyne (β-GDY) on a copper foil by the modified Glaser–Hay coupling reaction. Recently, Cui's group[7] synthesized a γ-graphyne (γ-GY) by a mechanochemical route through a solid–solid interfacial reaction between CaC_2 and hexabromobenzene.

Compared with graphene, the carbon atoms of GYs form much larger voids, and their electronic structures are also more abundant, which can synthesize GYs with various electronic configurations and aggregation structures. By changing the connection order of the C=C and C≡C bonds, GYs can also derive carbon materials with other electronic configurations, as shown in Fig. 2, which form parts of the GY family, such as α-GYs, β-GYs, δ-GY,[8] 6,6,12-GY,[9] and rhombic-GY.[10] However, γ-GDY and γ-GY are still the most studied GY structures because they were synthesized first and their preparation techniques are relatively mature. On the basis of the successful preparation of

[a]College of Sciences, Institute for Sustainable Energy, Shanghai University, Shanghai 200444, P. R. China. E-mail: hongbinzhao@shu.edu.cn; daixinye@shu.edu.cn; jiujun.zhang@i.shu.edu.cn

[b]University of Western Ontario, London N6A 5B8, Canada

† These authors contributed equally.

This journal is © The Royal Society of Chemistry 2020

Published on 30 September 2020. Downloaded by University of Western Ontario on 1/24/2021 7:05:58 PM.

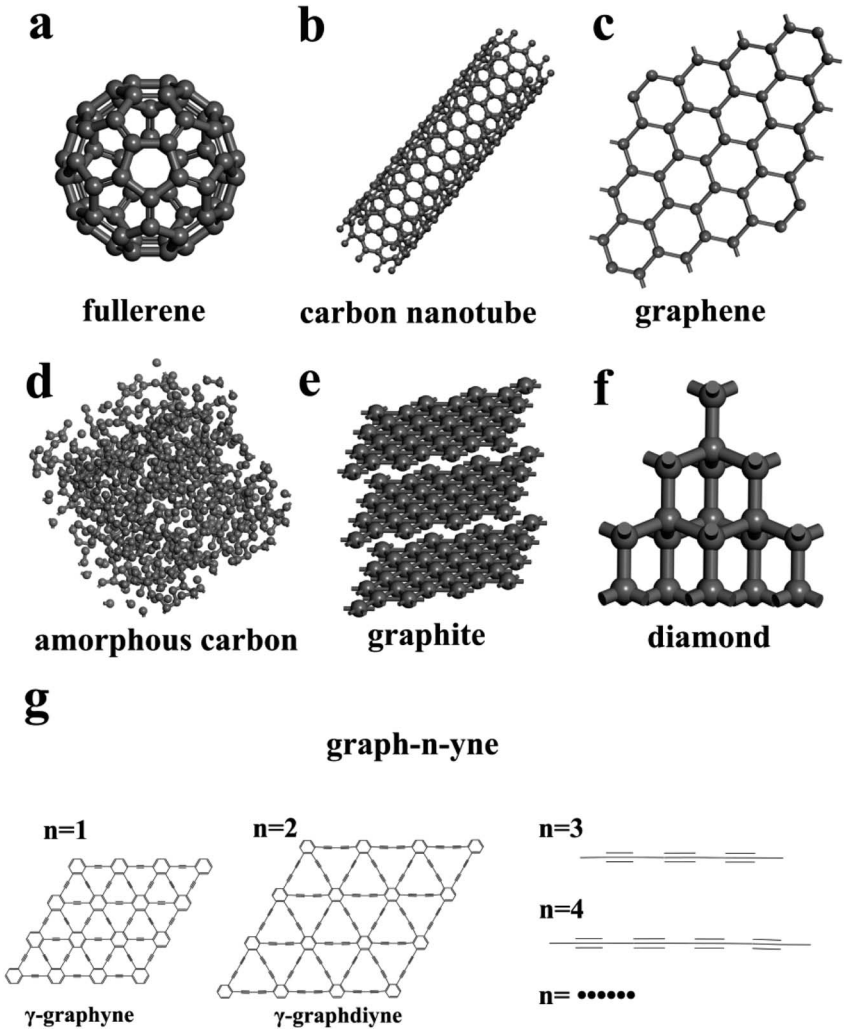

Fig. 1 Structures of different carbon materials. (a) Fullerene; (b) carbon nanotube; (c) graphene; (d) amorphous carbon; (e) graphite; (f) diamond; (g) GYs.

GDY, a lot of research work has been done, including the development of synthetic methods for GDY, the preparation of GDY with different aggregation structures and the modification GDY by doping.

1.2 Growth and doping mechanisms of GYs

GYs are sp- and sp^2-hybridized full carbon network structures formed by binding benzene rings to acetylene bonds. The distribution of the sp-C (C^1) atoms and sp^2-C (C^2) atoms is shown in Fig. 3a, and C^1 can be divided into αC^1 and βC^1 according to their positions. The growth mechanism of GYs is essentially a cross-coupling reaction of precursors containing benzene ring and acetylene bond structures. In the process, the terminal alkynes of the precursor bind to the catalyst of the Cu complexes, and the reaction can occur between the bound Cu complexes, which makes the terminal alkynes cross-coupled together in an orderly way to obtain GDY.[11] The GDY with corresponding morphology is formed on the surface of the template with different morphologies. γ-GY can be synthesized without catalyst. By the mechanochemical method, the crystal structure and molecular bond of the precursor CaC_2 are destroyed, resulting in a large number of $[C{\equiv}C]^{2-}$ and Ca^{2+}. The alkynyl groups (–C≡C–, with negative electricity) have high surface energy and reaction activity, which can be used as a nucleophile. It is thus easy to attack the carbon atom on the opposite position of the aromatic ring (with positive electricity) on the precursors by providing the aromatic ring (PAR), and form a C–C bond between them to result in an alkynyl substitution reaction. Due to the electron-withdrawing effect of the alkynyl group,[12] the partially substituted PAR still has a high nucleophilic substitution activity. The nucleophilic substitution reaction can continue until all other atoms on all PAR are replaced by the acetylenic group, resulting in a large area of 2D γ-GY.[7,13–15]

Usually, there are two methods in the preparation of the doped GDY. One is the use of the prepared GDY to react with the heteroatoms containing materials by a thermal synthesis method. At high temperature, the heteroatom free radicals from the heteroatom source decomposition can react with the

Published on 30 September 2020. Downloaded by University of Western Ontario on 1/24/2021 7:05:58 PM.

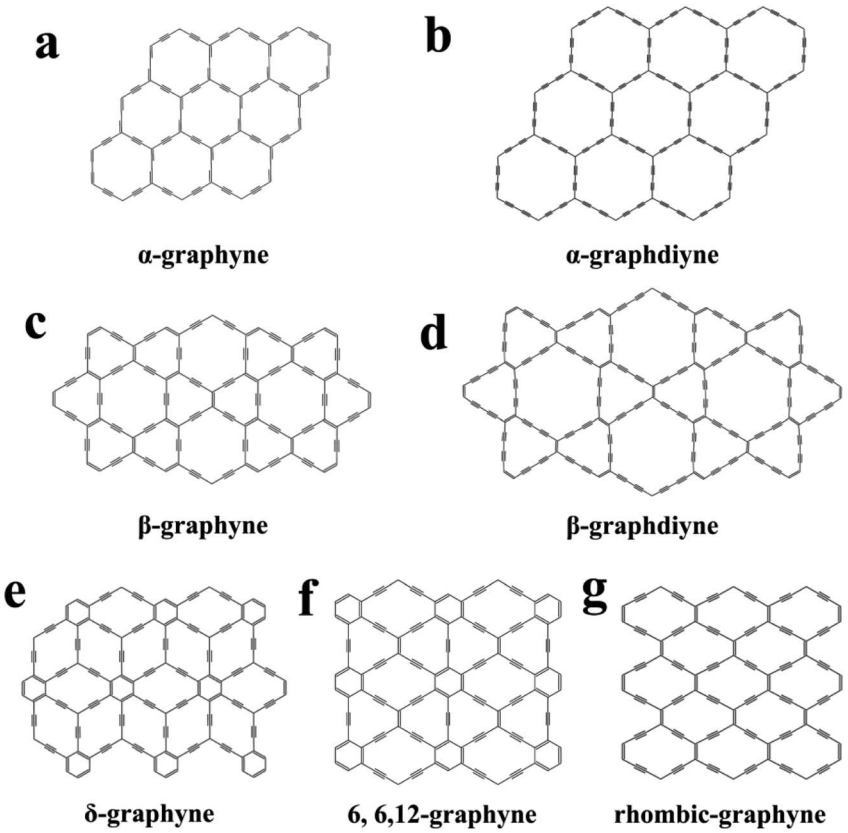

Fig. 2 Structure of other GY family members.

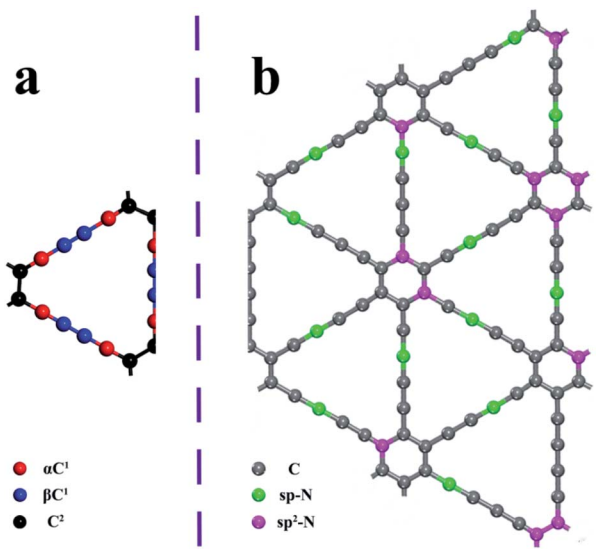

Fig. 3 (a) Types of carbons in pristine GDY (red: αC^1; blue: βC^1; black: C^2). (b) The position distribution of different N doping in GDY.

acetylenic bonds of GDY to form the C–heteroatom–C bonds of GDY, or directly substitute the hybridized C atoms in GDY to obtain the doped GDY, such as S-GDY,[16] N-GDY,[17,18] and Co–N-GDY.[19] As shown in Fig. 3b, N atoms can replace C atoms to complete the doping process. The other way, called the bottom-up process, directly uses the heteroatom-substituted precursors to prepare doped GDY by the cross-coupling reaction, which is similar to the preparation mechanism of pure GDY.[20–22]

1.3 Functional mechanisms of GY applications in energy storage and conversion

Electrochemical technologies (such as fuel cells, batteries, supercapacitors, and water electrolysis to produce hydrogen) have been recognized as the most efficient, reliable and practical options for energy storage and the conversion of electricity energy.[23–27] In these electrochemical energy technologies, all carbon materials shown in Fig. 1 have been widely used either for electrode materials or electrocatalysts. The unique structures of GYs have been demonstrated to multifarious glorious performances. It is also necessary to study the functional mechanisms in the field of energy conversion and storage, which is conducive to improving the performances of GYs.

In GDY, the C^1 atoms possess a positive charge and the C^2 atoms have a negative charge. The positively charged C^1 atoms can effectively adsorb O_2 to speed up reaction processes, such as the oxygen reduction reaction (ORR), making them excellent catalytic active sites in electrochemical catalysis.[28] As shown in Fig. 4a, the conjugated structures of GDY can facilitate electron transfer, while the pore structure is beneficial to the transportation of gaseous products, which can facilitate the electrocatalytic process, such as oxygen reduction reaction (ORR). For doped GDY, the introduction of heteroatoms can change the

 This journal is © The Royal Society of Chemistry 2020

Published on 30 September 2020. Downloaded by University of Western Ontario on 1/24/2021 7:05:58 PM.

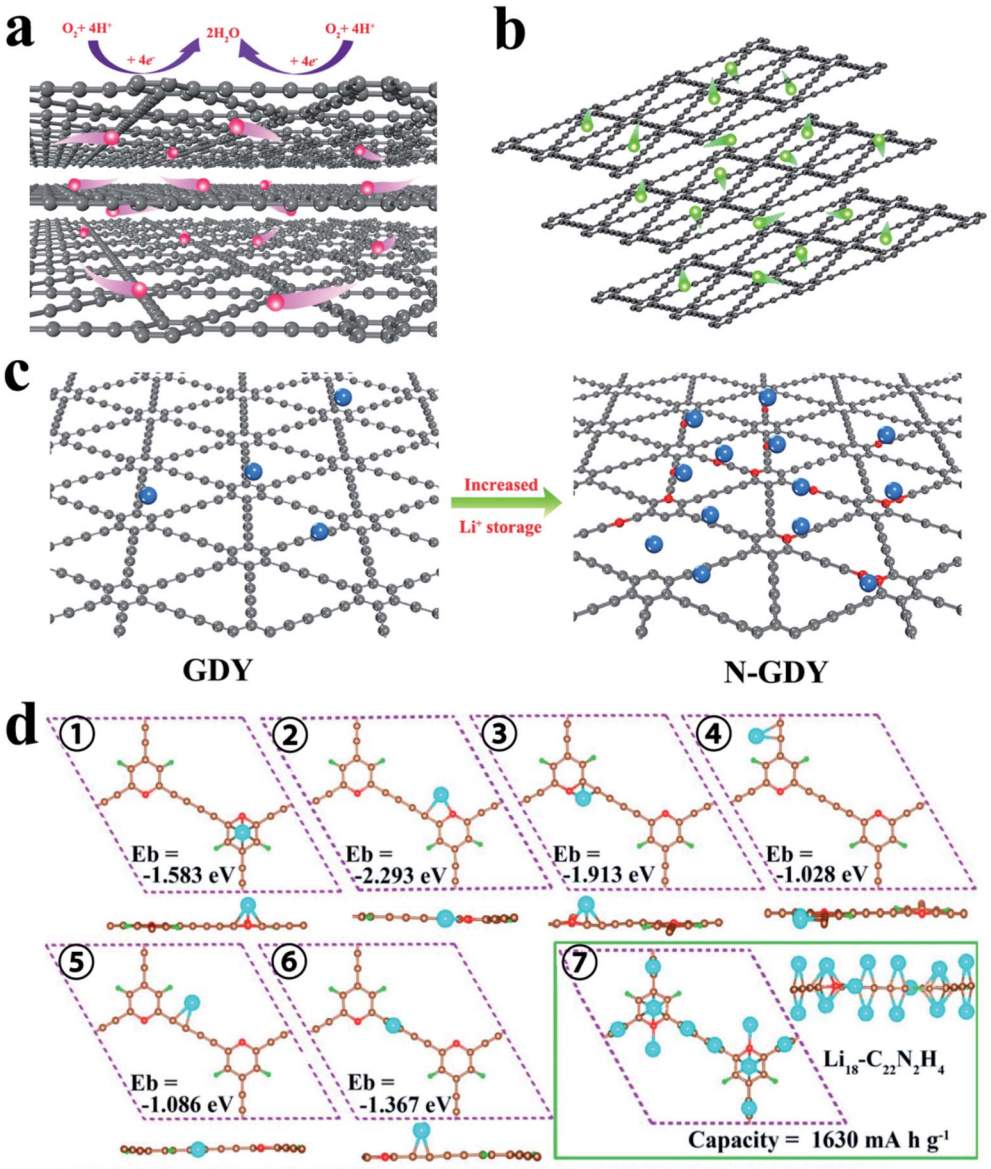

Fig. 4 (a) Schematic diagram of the role of the GDY electrocatalyst in the high ORR activity and intra-plane electron transfer. (b) Schematic diagram of the rapid transfer of ions at GDY in batteries and supercapacitors. (c) Schematic diagram of Li^+ storage in GDY and N-GDY (for panels a–c, gray: C; pink: electrons; green: ions; blue: Li^+; red: N; orange: H). (d) The adsorbable position of Li in PM-GDY (①–⑥), and the geometries of the optimized Li_{18}–$C_{22}N_2H_4$ complexes (⑦) from top and cross-section view. (d) Reproduced with permission.[32] Copyright 2018, American Chemical Society.

electron arrangement of GDY, and the number of active sites in the catalytic reaction can be increased by the formation of heteroatom defects.[29] Because of the presence of chemical bonds, the heteroatom active sites with atomic levels are uniformly and stably fixed on GYs. In a case study of N-GDY as the ORR catalyst by Density Functional Theory (DFT) calculations, the excellent ORR catalytic activity of the N-GDY could only be derived from single βN^1 (N replaced βC^1) doping and some βN^1 and N^2 (N replaced C^2) co-doping. Due to the co-existence of N^1 and N^2, the ORR activity of N-GDY (Fig. 3b) is close to Pt-based materials, which can be attributed to the synergistic effect between N^1 and N^2.[28]

The GYs have higher charge carrier mobility than graphene, the diffusion of electrons and ions on the surface of the GYs-based electrode can be significantly accelerated for the enhancement of electrochemical performance.[30] When GYs are used as the anode materials in lithium/sodium ion batteries (LIBs/SIBs), the storage and transfer mechanisms of Li/Na are the same as the anodes of other materials, and Li/Na ions are repeatedly embedded and removed between the positive and negative electrodes. Due to the unique electronic structure of GYs, they can exhibit high specific capacity and cycling stability in the batteries. The expanded in-plane pores surrounded by the butadiyne linkers and benzene rings in the structure of GDY can offer spaces for the rapid storage and diffusion of metal atoms.

Published on 30 September 2020. Downloaded by University of Western Ontario on 1/24/2021 7:05:58 PM.

For instance, Li^+ and Na^+ in batteries and supercapacitors[31] can diffuse in both parallel and vertical directions to the plane of GDY, as shown in Fig. 4b. When Li^+ intercalates into GDY, it is possible to form LiC_3. For doped GDY, there is a synergistic effect between the heteroatoms and GDY. Heteroatoms can change the electronic configuration of GDY and improve its electrochemical performance. At the same time, GDY can not only act as the carrier of heteroatoms, but also prevent the agglomeration of heteroatoms by chemical bonding between GDY and heteroatoms. The doping heteroatoms (such as N and F) can fabricate a lot of heteroatomic defects due to their electronegativity, which can provide more electrochemical active sites for Li^+ storage,[32,33] as shown in Fig. 4c. To further illustrate the effect of heteroatom doping on Li storage, for example, Yang *et al.*[32] explored pyridine-graphdiyne (PY-GDY), obtained the sites that Li atoms could adsorb on and the optimized binding energy (E_b), and the theoretical capacity were obtained by DFT calculation (Fig. 4d). The E_b of Li adsorbed near N (①–③) are larger than that adsorbed at other sites (④–⑥). E_b is closer to the N atom, and Li shows a higher E_b (②), indicating that the Li atoms adsorbed near N are more stable than the farther positions. Due to the lone pair electrons in the sp^2 orbit of pyridinic N, the electron clouds in the plane of the C skeleton are higher than those that are out of plane, so the E_b of ⑥ is larger than those for ④ and ⑤. Based on the calculation results of Li adsorption information, the theoretical capacity of PY-GDY using the optimized complexes of Li_{18}–$C_{22}N_2H_4$ (⑦) to estimate is 1630 mA h g^{-1}, and is higher than that of pure GDY.[34]

All of these excellent properties have made GYs the candidate materials for many applications, particularly in catalysis[35–37] and energy storage.[34,38]

To facilitate further research and development, in this review, we have summarized the current progress in electrochemical energy related GYs and GYs-based materials, including the heteroatom-doped GYs, the materials with GYs as carriers and the composites containing GYs, in terms of the advanced synthesis, heteroatom doping, functional mechanisms and applications. Moreover, several challenges hindering the practical applications of such GYs materials are summarized and analyzed, and the possible future research directions for overcoming the challenges are also proposed in this review.

2. Typical synthesis routes of GYs with controllable morphologies

GYs as a new kind of carbon materials have excellent physical and chemical properties. So far, there are many methods to synthesize GYs, and many different aggregate structures have been obtained. In this section, we will review and analyze the preparations of various aggregate structures of GYs.

Since the successful synthesis of GDY, its synthesis routes have been constantly innovative. The synthesis methods can be roughly divided into two categories: dry chemical method (explosion approach[20,39,40] and chemical vapor deposition (CVD) method[41]) and wet chemical method (Cu substrate method,[5,34,42–45] arbitrary substrate method,[46–48] template method,[49–51] solution-phase van der Waals epitaxial method,[52] interface method,[53,54] vapor–liquid–solid (VLS) growth method[55,56]). In addition, the mechanochemical method[7,13,14] can be also used to prepare γ-GY in both dry and wet environments. We have also investigated the literature regarding the application of GYs, and found that most of them are derivatives of GYs doped with other elements, so we will review different types of doped GYs.

2.1 Template-assisted aggregation structure regulation

The aggregation structures of materials have a great influence on properties. At present, the synthesis of GYs with a specific and desired morphology is still challenging. In the process of exploration, templates are widely used in various preparation methods of GYs. In this section, we will introduce the influence of templates on the adjustment of aggregate structure in the synthesis of GYs, and some related aggregation structures are shown in Fig. 5.

2.1.1 Cu substrate method. The Cu substrate method is the most classic method for preparing GDY using copper materials like Cu foil,[5,6,43,44,57] foam[42] and nanowires[34] as templates and the sources of catalysts. GDYs grow on the surface of the Cu substrate, and the aggregate structures of the resulting GDYs are controlled by the morphology of the Cu substrate. In the cross-coupling reaction, a small amount of Cu ions could be produced on the surface of the Cu substrate in the pyridine solution, which formed a pyridine–copper complex.[5,34,42] Under the catalysis of the pyridine–copper complex, the precursor formed GDY on the Cu substrate by the orderly cross-coupling reaction. Yang *et al.*[57] used Cu foil as the catalyst and template substrate to prepare the ultrafine pyrenyl graphdiyne (Pyr-GDY) nanofibers (Fig. 5a) with diameters of 3–10 nm. Huang *et al.*[43,44] used some Cu foils as sacrificial templates to prepare hierarchical porous GDY nanowalls, which were grown along the vertical direction of the Cu foil to form a loose porous nanostructure with abundant open voids (Fig. 5b and c). Shang *et al.*[34] used Cu nanowires as a catalyst source and template to prepare GDY nanotubes and nanosheets by controlling the amount of monomer HEB.

2.1.2 Arbitrary substrate method. The arbitrary substrate method can cleverly encapsulate other substrates into a copper foil. When the active Cu catalyst is transferred to other substrates, the *in situ* growth of GDY on other templates can be achieved. Wang *et al.*[47] used an Al template inside the Cu foil envelope and HEB as a precursor to successfully synthesize the ultrathin GDY film-decorated Al foil (Al-GDY). As shown in Fig. 5d, the sectional view of the Al-GDY foil with an unsharp interface and the ultrathin GDY layers with thickness less than 10 nm are conformally coated on the Al foil. They[48] also used a polypropylene separator as a template for the *in situ* preparation of GDY nanosheets through the Cu envelope.

2.1.3 Template method. In order to get the target morphology, the template method plays a very important role. Li *et al.*[50] used an anodic aluminum oxide template to synthesize the GDY nanotubes. The surface was smooth and the wall thickness was nearly 15 nm (Fig. 5e and f). Li *et al.*[49] used low-

 This journal is © The Royal Society of Chemistry 2020

Published on 30 September 2020. Downloaded by University of Western Ontario on 1/24/2021 7:05:58 PM.

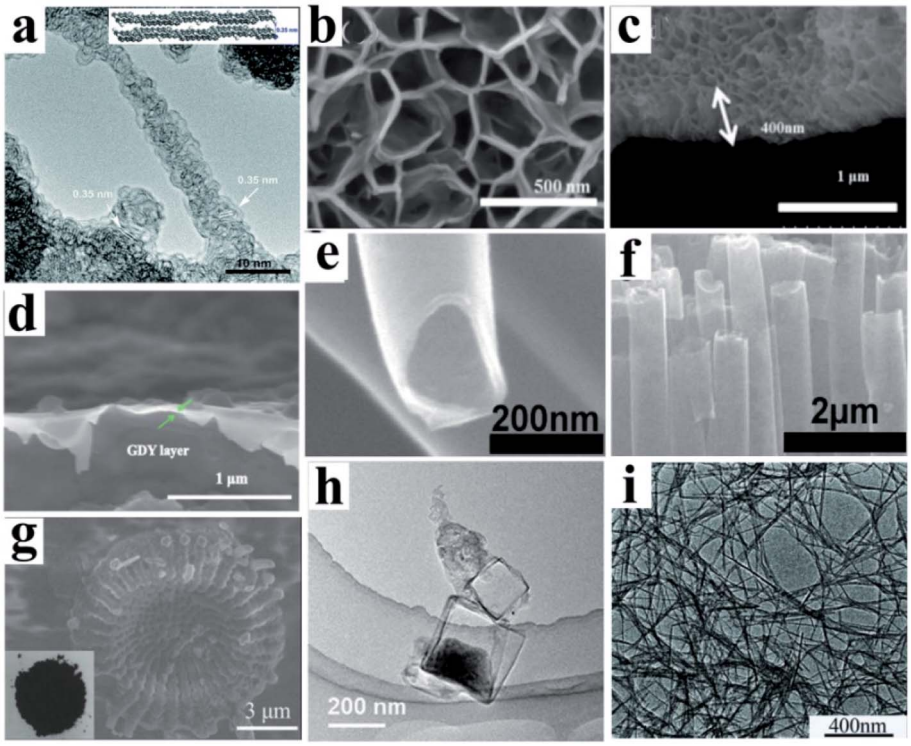

Fig. 5 Aggregate structures of GDYs by regulating synthetic conditions. (a) TEM images of Pyr-GDY, showing a single Pyr-GDY nanofiber with an interlayer spacing (*d*-spacing) of 0.35 nm (inset a). Adapted with permission.[57] Copyright 2019, the Royal Society of Chemistry. (b) Top view SEM images of GDY nanowalls on Cu substrate and (c) cross-sectional view of GDY nanowalls as an exfoliated sample. (b and c) Adapted with permission.[44] Copyright 2017, Elsevier Ltd. (d) Cross-sectional view of the morphology and structure for GDY-decorated Al anode. Reproduced with permission.[47] Copyright 2019, Elsevier Ltd. (e) Top view SEM image of GDY nanotube and (f) side view TEM image of a GDY nanotube array. (e and f) Adapted with permission.[50] Copyright 2011, American Chemical Society. (g) SEM image of 3D GDY. Adapted with permission.[49] Copyright 2018, Wiley-VCH. (h) TEM image of cuboidal GDY films. Reproduced with permission.[58] Copyright 2020, Wiley-VCH Verlag GmbH & Co. KGaA, Weinheim. (i) Low magnification TEM image of GDY nanowires. Adapted with permission.[55] Copyright 2012, the Royal Society of Chemistry.

cost diatomite as the template and Cu nanoparticles as the catalyst to synthesize the round cakelike 3D GDY (Fig. 5g), which had a large specific surface area and the interior was connected by hollow GDY columns. Wang *et al.*[51] also reported similar work that successfully produced GDY stripe arrays.

2.1.4 Interface method. Using the interface as a template is a feasible method to prepare 2D few-layer GDY.[53,54] By controlling the contact area between the reaction substrate and the catalyst at the liquid/liquid or gas/liquid interface, and using the interface as the template, the 2D GDY layers were formed by the catalytic coupling reaction. Zhang *et al.*[59] prepared a cyano-functionalized graphdiyne (CN-GDY) by this interface method, which was a well-defined crystalline film with an average thickness of 4.3 nm. Yin *et al.*[58] reported a microwave-induced temperature gradient at a solid/liquid interface to prepare a few-layer GDY. In the process, using the solid/liquid interface of the NaCl crystal surfaces and toluene/hexane solution as templates, the HEB monomers could lead to the formation of ultrathin GDY films by the cross-coupling reaction on the surface of NaCl, as shown in Fig. 5h.

2.1.5 VLS growth process. The VLS growth process could construct the GDY nanowires[55] and thin films with different layers[56] using ZnO nanorod arrays on a silicon slice as a substrate through a VLS mechanism.[60,61] Qian *et al.*[55] used the VLS method to successfully synthesize GDY nanowires, which were about 300 to 700 nm in length and about 20 to 30 nm in diameter (Fig. 5i), and exhibited a high-quality flaw-less surface. They also synthesized 2D GDY films through a combination of reduction and a self-catalyzed VLS growth process.[56]

2.1.6 Van der Waals epitaxial strategy. Due to the alkyne–aryl single bonds in GYs, they can rotate freely. The thickness of the synthetic GDY layer is difficult to control. In particular, the controllable synthesis of GDY with single or few layers is still a challenge. Gao *et al.*[52] synthesized an ultrathin single-crystalline GDY film at room temperature using the solution-phase van der Waals epitaxial strategy with 2D graphene as the template. The thickness of the GDY films continuously grown on the graphene template was only 1.74 nm, including the monolayer graphene.

2.1.7 CVD method. In the dry chemical method, the CVD method as an attractive and common synthetic strategy has been widely used in preparing 2D materials. Liu *et al.*[41] used Ag foil as a template and HEB as a precursor to prepare the homogeneous monolayer GDY by CVD method. They indicated that the surface-assisted process could control the growth of carbon networks. Although the CVD method can prepare a single layer GDY, the crystallinity and thickness control of GDY still need to be improved.

Published on 30 September 2020. Downloaded by University of Western Ontario on 1/24/2021 7:05:58 PM.

It is the most direct and effective synthetic strategy using templates to assist in the synthesis of the desired aggregate structures. During preparation, the selection of the template and the monomer concentration are critical in the structural control of the nanoscale GYs.[30] However, this template strategy still has a long way to go in terms of the mass and precision production of a specific aggregation structure of GYs.

2.2 Polar solvents-assisted etching for GDYs quantum dots

In general, a system of carbon quantum dots (QDs) is constrained by 3D direction and has a more obvious quantum effect, which has unique optical properties and high biocompatibility.[62,63] As early as 2014, Zhang *et al.*[64] studied GY QDs by applying the first-principles calculations.

In order to obtain the GDY quantum dots (GD QDs), the researchers have used polar organic solvents to assist in etching the existing GDY. Zhang *et al.*[65] treated the existing GDY in chlorobenzene (CB) or dimethylsulfoxide (DMSO) solution by ultrasonic treatment and stirring, and then GD QDs were obtained in the supernatant. The architecture and TEM image of the GD QDs are shown in Fig. 6a and b, in which the QD sizes of 3–5 nm were well-distributed. The inset in Fig. 6b shows the GD QDs fabricated with different solutions to research the influence of the polarity of the solution on the preparation of GD QDs. Min *et al.*[66] first treated graphdiyne oxide nanosheets with a hydrothermal method, followed by ultrafiltration and dialysis, and got the GD QDs (Fig. 6c). The size distribution was narrow and the average diameter was about 4.21 nm (Fig. 6d).

In the preparation of some 2D QDs materials,[67–69] GDYs are found to be easily dispersed to be nanosheets in polar solvents and further etched to be GD QDs, which may be the only way to prepare GD QDs as reported so far. There are many similarities between graphene and GDYs, and the graphene QDs can be obtained by many methods.[70–73] So, it is possible to learn the preparation method of graphene QDs to obtain GD QDs.

2.3 Defect/substitution regulated conjugated skeleton of GYs

In general, according to the type and distribution of carbon atoms, the materials will show different electrical conductive behaviors.[74–76] Doping modifications can greatly improve the GYs' electronic and catalytic properties due to the heteroatom defects having a great impact on the physical and chemical properties of GYs, such as electrical resistance, surface chemical activity, and chemical energy. In this section, we will review and analyze how to modify the conjugated skeleton of GYs by doping heteroatoms to replace the carbon atoms to generate defects in the structure.

2.3.1 GYs doped with non-metallic atom. Doping modification is a fast and effective way for the preparation of high-performance materials. Due to the electronegativity difference of carbon and the heteroatom, the doping heteroatoms (B,[78–80] Si,[81] N,[20,77,82] P,[80] S,[16] F,[83] and Cl[81]) can improve the surface chemical activity of the GYs, and also adjust the electronic structures.

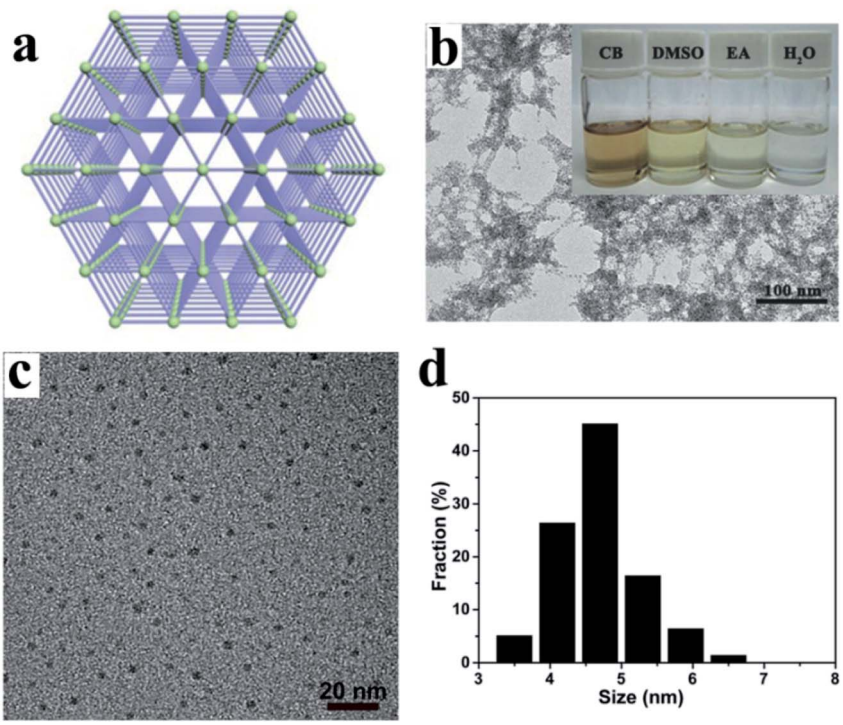

Fig. 6 (a) GD QDs architecture of GDY; (b) TEM image of dispersed GD QDs. The inset is a photograph of GD QDs fabricated with different solutions: ⟨CB, DMSO, ethanol (EA), and H_2O⟩. (a and b) Reproduced with permission.[65] Copyright 2017, Wiley-VCH Verlag GmbH & Co. KGaA, Weinheim. (c) TEM image of GD QDs. (d) Size distribution of GD QDs. (c and d) Reproduced with permission.[66] Copyright 2019, American Chemical Society.

 This journal is © The Royal Society of Chemistry 2020

Published on 30 September 2020. Downloaded by University of Western Ontario on 1/24/2021 7:05:58 PM.

According to the latest experimental progress, Mortazavi *et al.*[80] predicted the N-, B-, P-, Al-, As- and Ga-GYs 2D lattices by using DFT calculation. The electronic structure analysis showed that the predicted monolayer GYs had semiconductor electronic properties. Felegari *et al.*[84] studied the effect of B, N, Si and other atoms on the adsorption activity of GY for phosgene using DFT calculation. Each atom (B, N, and Si) was substituted for the carbon atom in the aromatic core of doped GY. The electron disturbance induced by doping atoms, especially Si, could enhance the sensitivity of GY to phosgene adsorption. Ma *et al.*[77] used DFT to calculate the N 1s spectra of N-doped GDY. They presented five N-doped GDYs, which are amino, pyridinic, graphitic and two sp-hybridized N (sp-N-1 and sp-N-2), whose properties were entirely calculated, and their local structures are shown in Fig. 7a. Their work provided the fundamental references for the structural determination of the N-doped GDY, and a new comprehension of the potential structure–property relationships. Huang *et al.*[16] proposed using an organic sulfur source to prepare a S-GDY powder for further improving the properties of GDY. The preparation process is shown in Fig. 7b. The presence of S atoms in a unitary modality of the C–S–C bonds could increase the number of active sites and defects of GDY, thus enhancing the electrochemical performance of S-GDY. Xiao *et al.*[83] reported that using F elements to modify GDY (F-GDY) was a feasible route to coordinate its distinct structure and photoelectronic capabilities. Three steps occurred in the process of preparing F-GDY: the breaking of acetylenic bonds, partially fluorinating C–F having covalent bond with

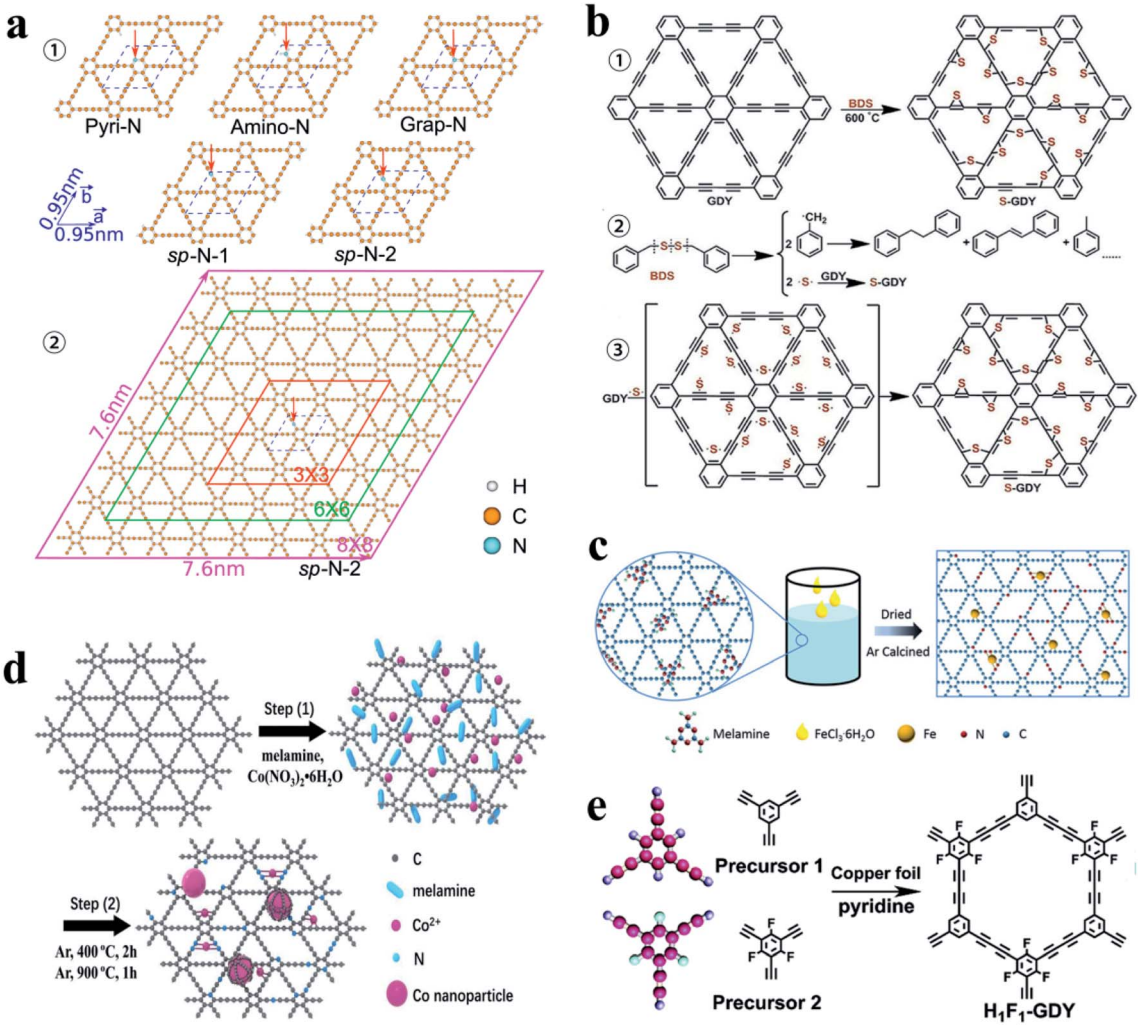

Fig. 7 (a) Periodic structural models: ① local structures of five different nitrogen doping types: Pyri-N, Amino-N, Grap-N, sp-N-1 and sp-N-2. Unit cell is illustrated by blue dashes. ② Different sizes of supercells of N-doped graphdiynes (3 × 3, 6 × 6, 8 × 8) for sp-N-2. Low doping concentration is assumed in this work, and the doped cell is always surrounded by pristine GDY cells. Nitrogen positions are labeled by arrows to guide eyes (a colour version of this figure can be viewed online). Reproduced with permission.[77] Copyright 2019, Elsevier Ltd. (b) ① Schematic illustration of the preparation of S-GDY by using a simple thermal synthetic. ② Heat-transfer mechanism of S atoms in benzyl disulfide (BDS). ③ Proposed reaction intermediate for the chemical modification of the sp-hybridized carbon atoms of GDY. Reproduced with permission.[16] Copyright 2019 Wiley-VCH. (c) Schematic illustration of the synthetic procedure for Fe–N-GDY catalysts. Reproduced with permission.[11] Copyright 2019 Wiley-VCH. (d) Schematic illustration of the preparation of Co–N-GDY. Reproduced with permission.[19] Copyright 2019, Elsevier Ltd. (e) The schematic diagram of the preparation for H_1F_1-GDY, and the ball-and-stick model of two precursors. Reproduced with permission.[22] Copyright 2020, Elsevier B.V.

Published on 30 September 2020. Downloaded by University of Western Ontario on 1/24/2021 7:05:58 PM.

GDY hybridizing with regional sp^2-carbon. Kang *et al.*[85] also prepared the F-GDY film with a thickness of 610 nm by a similar method.

The directly synthesized doped GYs can achieve heteroatoms uniformly distributed on GYs. Zhang *et al.*[86] prepared a hydrogen-substituted graphyne (HsGY) film on the gas/liquid interface using 1,3,5-tripynylbenzene (TPB) as a precursor through the alkyne metathesis reaction. Li *et al.*[21] reported the design and synthesis of a highly crystalline benzene-substituted graphdiyne (Ben-GDY) using the supramolecular chemistry method. Ben-GDY had a multilayer structure due to the introduction of π–π/CH–π interactions to control the conformations of precursors in the preparation process.

2.3.2 GYs doped with metallic atom. Recently, the interaction between the metal atom with graphene and that between the metal atom with GYs have been studied by theoretical calculation. The results point out that the metal atom with GYs is a strong chemical adsorption, while the metal atom with graphene is a classical physical adsorption.[87,88] This indicates that there is a strong charge transfer between the metal atom and GYs, and the doping of the metal atom can effectively regulate the electronic and magnetic properties of the GYs. Thus, the properties of GYs can be modified, providing a basis for its application in electronic devices. Gangan *et al.*[89] studied an yttrium-doped GY (Y-GY) by the first-principles DFT calculations and molecular dynamic simulation of its hydrogen storage capacity. They found that the synergistic effect of the acetylene linkage and yttrium in Y-GY played an important role in improving the hydrogen storage capacity.

2.3.3 GYs co-doped with two types of atoms. In two or more heteroatoms co-doped GYs, there is a synergistic effect between the heteroatoms and GYs and even between heteroatoms. This makes the co-doped GYs have better performance than pure GYs. Akbari *et al.*[90] studied the effect of single atom N or Al doping and Al–N co-doping GY on the hydrogen storage performance by DFT method. The capacity to store hydrogen and the structural and electronic properties of the co-doped GY were effectively enhanced, which in turn, had the synergistic effect on the adsorption of hydrogen. Si *et al.*[11] prepared a Fe & N co-doped graphdiyne (Fe–N-GDY), as shown in Fig. 7c. The GDY, Fe and N together in the Fe–N-GDY catalyst have a vital synergistic effect for enhancing stability and catalytic performance. Wang *et al.*[19] designed and synthesized a novel electrocatalyst of Co & N co-doped GDY (Co–N-GDY), as shown in Fig. 7d. The N-doping can change the electronic configuration of GDY, and the bonding effect between GDY and Co nanoparticles can make the high Co content in Co–N-GDY. For example, Lu *et al.*[22] prepared H, F evenly co-substituted GDY (H_1F_1-GDY) (Fig. 7e), which was achieved by controlling the amount of precursor containing heteroatoms to be doped. The opposite electronegativities of H and F could facilitate the formation of interfacial stable nanostructures.

When GYs are doped with a heteroatom, the carbon on the carbon network will be replaced by heteroatoms. The formed heteroatom defects in the position of substitution or the heteroatoms are bonded to the GYs with the carbon–carbon triple bonds as the binding sites. The heteroatom doping can affect the properties of GYs by changing their electronic configuration, and increasing the number of active sites and heteroatom defects.

2.4 The expected method for large-scale production of GYs

GYs are a kind of carbon materials with infinite application potential. However, compared with graphene, the production quantity of GYs obtained by most of the preparation methods is very small, which brings large obstacles to the extensive research and application of GYs. Here, we will summarize some synthesis ways, which have the potential for preparing GYs in a large scale.

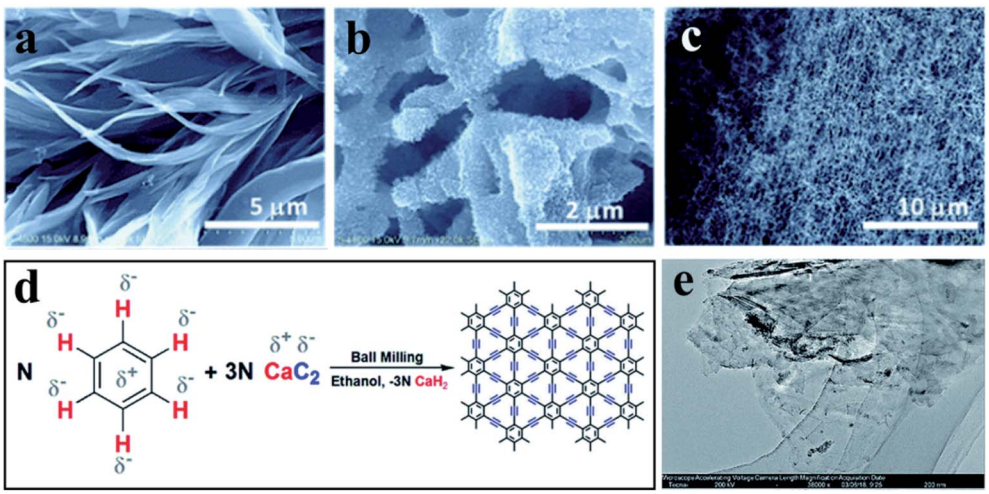

Fig. 8 The SEM images of (a) the GDY ribbons, (b) the 3D framework of GDY and (c) the GDY nanochains, which were prepared by explosion approach. (a–c) Reproduced with permission.[40] Copyright 2017, the Royal Society of Chemistry. (d) Schematic illustration of the reaction pathway for the preparation of γ-GY; (e) the TEM image of γ-GY. (d and e) Reproduced with permission.[14] Copyright 2019, the Royal Society of Chemistry.

 This journal is © The Royal Society of Chemistry 2020

Published on 30 September 2020. Downloaded by University of Western Ontario on 1/24/2021 7:05:58 PM.

2.4.1 Explosion approach. Based on the Glaser–Hay coupling reaction with noble metal surface in solution, Zuo *et al.*[40] reported the explosion approach, which was a time efficient method to prepare GDY with large quantities in the atmosphere. By controlling the reaction temperature and gas atmosphere, they obtained GDYs with three different aggregate structures (Fig. 8a–c). Wang *et al.*[39] improved the explosion approach to get 3D ultrafine GDY nanochains on nickel foam. Using the explosion approach, due to the absence of toxic solvents and unnecessary special equipment, it has a great potential to be applied in mass production in the future.

2.4.2 Mechanochemical method. The mechanochemical method can obtain gram-scale γ-GY, which greatly enriched the preparation and knowledge of GYs. Cui's group[7,13] successfully prepared the γ-GY with a 2D structure by the ball milling and calcination processes using $PhBr_6$ and CaC_2 as the reactants. This γ-GY had a distinctive large conjugate structure and good Li^+ diffusion coefficient. They also used benzene and CaC_2 as precursors to prepare 2D γ-GY by ball milling, and the schematic diagram of the reaction process is shown in Fig. 8d.[14] The prepared γ-GY was layered with a perimeter of about 400 nm (as shown in Fig. 8e), and a thickness of about 0.7 nm. Ding *et al.*[91] prepared multilayered γ-GYs using $PhBr_6$ and CaC_2 as raw materials by ultrasound-promoted method, which was a simple and easy way in operating. However, the purity of the γ-GY prepared by the mechanochemical method is low, which also requires post-treatment work to remove impurities.

The realization of high quality and large-scale production is of great significance to the further development, research and application of GYs. However, there are still some deficiencies in the current methods. For example, the GDY without external pollution could be obtained by the explosion approach, but the reaction conditions are somewhat harsh. The reaction process was also too fast to control the crystallinity and aggregate structures of GDY. Although the mechanical method was simple, it could only prepare γ-GYs currently. Due to the impurity in the product, some post-treatment work is still needed. So, there are still lots of work we can do to improve the preparation methods of GYs.

In this section, we introduce the preparation methods of different aggregation structures, doping strategies with different elements and the large-scale preparation of GYs. The aggregation structure determines the performance of the material, so we have summarized the synthesis methods of GYs with different aggregation structures, as shown in Table 1. Graphene has achieved large-scale and high-quality production and commercial applications. Compared with graphene, the preparation technology of GYs is immature and needs to be further explored. Nevertheless, with the rapid progress of the GYs research, a method with controllable morphology and the corresponding mass production can be realized in the near future.

Table 1 Summary of the preparation method of GYs on aggregation structures

Morphologies	Methods	Ref.
GDY quantum dots	Ultrasonic treatment	65
	Solvothermal method	66
GDY nanotubes	Cu substrate	34
	Template method	50
GDY nanochains	Explosion approach	20,39 and 40
GDY nanofibers	Cu substrate	57
GDY nanowires	Cu substrate	92
	VLS	55
GDY ribbons	Explosion approach	40
	Liquid/liquid interface method	93
GYs films	Cu substrate	85,94 and 95
	CVD	41
	Solution-phase van der Waals epitaxy	52
	Liquid/liquid interface method	53 and 96
	Microwave-induced solid/liquid interface method	58
	VLS	56
	Alkyne metathesis reaction	86
GYs nanosheets	Cu substrate	34 and 47
	Mechanochemical method	7,13 and 14
	Gas/liquid or liquid/liquid interface method	54
	Arbitrary substrate method	48
	Ultrasound-promoted method	91
GDY nanowalls	Cu substrate	44 and 45
	Arbitrary substrate method	46
3D GDY	Cu substrate	42,43 and 49
	Template method	42 and 49
	Explosion approach	40
	Supramolecular interactions	21

Published on 30 September 2020. Downloaded by University of Western Ontario on 1/24/2021 7:05:58 PM.

3. Special structures of GYs and GYs-based materials determining their applications in energy conversion and storage

GYs are a class of 2D all-carbon molecules with carbon in sp and sp^2 hybrids. Because both carrier migration and heat diffusion are confined in the 2D plane, the 2D materials show peculiar properties.[97] The special structures of GYs determine their unique physical and chemical properties, such as non-uniformly distributed electronic structure, moderate and adjustable band gaps,[98] high carrier mobility,[30] high conjugated structure[13] and uniformly distributed pores.[99] These advantages mean that GYs with 2D structures should have good applications in electronic information, environment, biology, energy storage and conversion, catalytic and other fields. For example, GYs are a type of n-type semiconductor with suitable bandwidth. The theoretical calculation shows that the electron cloud density of GYs is higher than that of graphene. Pure graphene is a zero-band gap material, in contrast, monolayer GDY has intrinsic proper band gap of 0.5 eV and high electron mobility.[100,101] So, GYs as a promising semiconducting material can used in nanoscale devices, such as field effect transistors (FETs),[102,103] and by calculating, GDY FET contacting with metals have high current on-off ratio of 10^4 and large on-state current of 1.3×10^4 mA mm^{-1} in a 10 nm channel length.[104] Zhang *et al.*[102] reported a flexible GDY-based FET device which had a carrier concentration of about 10^{14} cm^{-3} and repeatable on/off ratio of more than 10^2. The effect of bending at different angles on the device performance is not obvious, which proved the potential of GDY-based materials as flexible electronic devices.

Although single or few layered 2D GYs have been synthesized and studied deeply in theory, they are unable to support themselves and are prone to aggregate when transferred to the substrate. The structure at the edge is unstable and prone to wrinkles and curls, resulting in parts of the GYs changing from 2D to 3D structure. Compared with the 0D and 1D materials, there is a much stronger interaction between 2D layers, which is achieved by intimate face-to-face stacking between layers to constitute a 3D structure.[105] There are strong van der Waals forces between the layers of the 2D materials, which require large mechanical or chemical forces to separate the layers.[106] In fact, there is not much practical value for 2D materials, because in practical applications, such as catalysis or energy storage, 2D materials will be self-assembled or stacked together to form 3D structural materials. Regarding this, the surface utilization rate of the stacked GYs needs to be explored significantly for further improving the catalytic activity, stability, and then electrochemical performance of GYs as the negative electrode materials of batteries or supercapacitors.

In the following subsection, we will discuss the latest research and development of GYs and GYs-based materials, and their applications in energy-related fields.

3.1 Application of GYs as a carrier

The unique electronic structures of GYs determine their great potential for applications in energy-related fields. To further improve the performance of GYs, researchers have modified them by preparing GYs with different structures and hetero-atom doping. In practical applications, GYs are also promising materials as carriers. The selection of a suitable carrier can adjust the particle size of the materials, and improve the effective utilization area. GYs as 2D carbon materials, which have special atomic arrangements and electronic structures, large specific surface areas and excellent electron transport performance, can be used as the carriers for providing a large number of active centers.

Pt is a transition metal element with empty 3d-orbital. If Pt nanoparticles are loaded on GDY, the chemical bond between Pt and GDY is easy to form, which can help improve the electron transport during catalysis.[109] Shen *et al.*[110] fixed Pt nanoparticles on the GDY carrier (Pt-GDY) *via* microwave-assisted distribution as a catalyst for hydrogenation, and showed both high stability and efficiency. The introduction of a GDY carrier could avoid the aggregation of Pt nanoparticles, and increase the interaction between the Pt nanoparticles and reactants. Pt-GDY showed fine X-ray absorption near edge structures (XANES) being similar to those of pure Pt foil, with the intensity of the "white lines" at 11.56 keV. These lines increased a little compared to that of the pure Pt foil, indicating an increase in the d-band vacancy. Compared with commercial Pt/C, such a Pt-GDY showed higher catalytic activity for the hydrogenation of aldehydes and ketones to alcohols. Yang *et al.*[57] synthesized Pd/pyrenyl graphdiyne (Pd/Pyr-GDY), and used it as a catalyst for the photocatalytic reduction of 4-nitrophenol. First, they used the 1,3,6,8-tetraethynylpyrene monomer on Cu foil to prepare the ultrafine Pyr-GDY nanofibers by a modified Glaser–Hay coupling reaction, and then mixed this Pyr-GDY into K_2PdCl_4 aqueous solution under vigorous stirring. After washing, Pd/Pyr-GDY was obtained, as shown in Fig. 9a. The photocatalytic activity of Pd/Pyr-GDY for the reduction of 4-nitrophenol was higher than commercial Pd/C and other samples, which was due to the "clean surface" of Pd and the unique 3D network structure of Pyr-GDY to instant mass transfer (Fig. 9b and c). As shown in Fig. 9d, Li *et al.*[107] prepared the atomic Pd on GDY/graphene heterostructure (Pd_1/GDY/G) by novel van der Waals epitaxy method and wet chemistry approach, and used Pd_1/GDY/G as the catalyst to catalyze the reduction of 4-nitrophenol. The results showed that this catalyst had both high stability and activity. The GDY/G heterostructure was found to play an important supporting role in stabilizing single atom catalysts. This study provided a development direction of GDY as a carrier for energy storage and conversion applications.

γ-GY is also an excellent carrier in applications, such as single-atom catalysts (SACs). Ni *et al.*[108] reported Cu single atoms supported on GYs (Cu-GYs), and then the effects of Cu-GYs on the catalytic activity for CO_2 electrochemical reduction by DFT calculations. As shown in Fig. 9e, the activity of Cu-GYs varied with the pore size of GYs, which directly determined the coordination numbers of the single metal atoms. Another factor

 This journal is © The Royal Society of Chemistry 2020

Published on 30 September 2020. Downloaded by University of Western Ontario on 1/24/2021 7:05:58 PM.

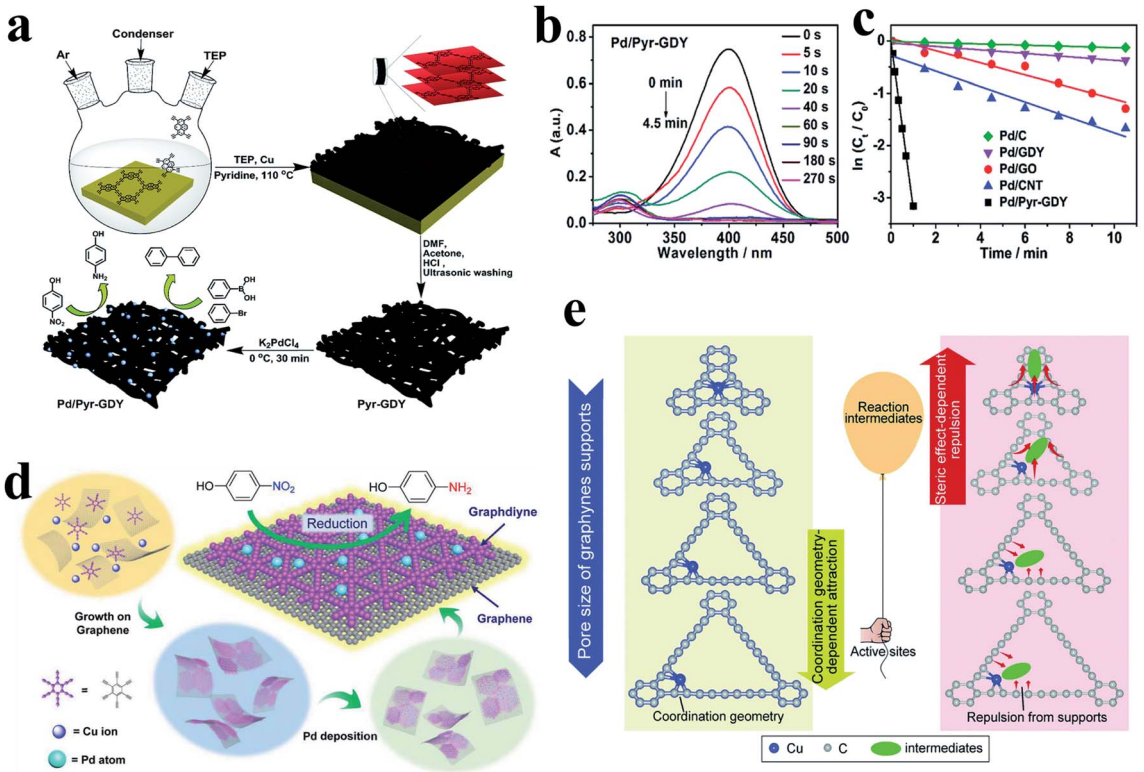

Fig. 9 (a) Preparation of the Pd/Pyr-GDY composite and its catalytic reactions. (b) Time-dependent UV-vis absorption spectra recorded during the catalytic reduction of 4-nitrophenol by Pd/Pyr-GDY. (c) Plots of $\ln(C_t/C_0)$ as a function of the reaction time for the reduction of 4-nitrophenol catalyzed by Pd/Pyr-GDY, Pd/GO, Pd/CNT, Pd/GDY and commercial Pd/C. (a–c) Adapted with permission.[57] Copyright 2019, Royal Society of Chemistry. (d) Schematic illustration of the experimental setup for GDY/G heterostructure synthesis through a solution-based van der Waals epitaxy method, Pd_1/GDY/G preparation and catalyzed for 4-NP reduction. Reproduced with permission.[107] Copyright 2019, Wiley-VCH. (e) Two influencing factors of the CO_2 electrocatalytic activity of GYs-supported Cu single atoms, adapted with permission.[108] Copyright 2020, Royal Society ofChemistry.

was the steric repulsion of reaction intermediates with the support skeleton of GYs. GYs with larger pores made them easier for reaction intermediates to access active sites. This study inspired people to pay more attention to the value of the carrier on the electrocatalytic properties of composite materials.

In this section, we have focused on several materials using GYs as the carriers, which will be further introduced in the following application parts. With the advancement of research, the mechanisms of GYs-based materials will be further studied and their applications will be more extensive.

3.2 Applications of GYs for catalysis

Catalysis as an important phenomenon in nature extensively exists in the whole field of chemical reactions. As a catalyst, there are three important indicators: activity, selectivity and stability. The GYs are composed of sp and sp^2 hybridized carbon with high π-conjugated structures. Density functional theory (DFT) calculations indicate that GDY can improve the water oxidation activity by changing the electron transport rate at the interface.[37] In this section, we will introduce the latest applications of GYs and GYs-based materials in catalysis.

3.2.1 Photocatalysis. Since Fujishima and Honda discovered in 1972 that the TiO_2 single crystal electrode can photocatalytically decompose water, more materials have been used as photocatalytic materials.[111] Due to its special electronic configuration and structure, GDY was also used in photocatalysis to compound with TiO_2 nanoparticles (P25) in 2012.[112] The chemical bonds were formed between the GDY and P25, which could reduce the energy band gaps of P25 and expand the range of light absorption.

GYs can be used as carriers and enhancers in photocatalytic reactions, which can be attributed to the characteristics of the 2D materials and special carbon–carbon bonds. Xu *et al.*[113] prepared a TiO_2/GDY network by electrostatic self-assembly method and studied its photocatalytic CO_2 reduction. The mechanism and properties of CO_2 photoreduction catalyzed by TiO_2/GDY were verified by DFT simulations, XPS and other characterization methods. The schematic diagram of the catalytic photoreduction of CO_2 is shown in Fig. 10a. Under the condition of UV-visible light irradiation, the catalytic activity of the TiO_2/GDY toward CO and CH_4 production was much higher than that of pure TiO_2, as indicated by Fig. 10b (TG*x* represents TiO_2/GDY, where T = TiO_2, G = GDY, and *x* was the weight percentage of GDY in TiO_2/GDY.). However, with increasing weight percentage of GDY in the catalyst, the yields of CO and CH_4 are increased first and then decreased. They thought that

Published on 30 September 2020. Downloaded by University of Western Ontario on 1/24/2021 7:05:58 PM.

the weak adsorption of CO was conducive to the production of CO. Through, DFT calculation, it was found that the adsorption energy of GDY for CO was small enough to be ignored, so that with increasing GDY content, the yield of CO was increased first. When the GDY content was further increased to a certain amount, the yield of CO began to decrease. The possible reason was that GDY hindered the absorption of TiO_2 to UV-visible light. Li *et al.*[115] used GDY with CdSe quantum dots (CdSe-QDs/GDY) as a photocatalyst material in a photoelectrochemical water splitting cell, which showed a high and stable performance. The function of GDY in CdSe-QDs/GDY was for as the hole transfer to enhance photocurrent. Li *et al.*[37] took into account the influence of GDY's surface wettability properties of, and prepared a composite material of superhydrophilic GDY and ultrathin CoAl-LDH (CoAl-LDH/GDY) by air-plasma treatment for electrocatalytic oxygen evolution reaction, and another material of superhydrophobic CoAl-LDH/GDY/$BiVO_4$ for photoelectrocatalytic reaction. As show in Fig. 10c–e, such a superhydrophobic CoAl-LDH/GDY/$BiVO_4$ has higher photocatalytic performance than others, demonstrating that the superhydrophilic GDY can improve the oxidation activity of water by promoting interfacial electron transport. Xu *et al.*[114] synthesized a novel GDY/graphic carbon nitride (g-C_3N_4) nanocomposites by a calcination method. Under visible light, this GDY/g-C_3N_4 showed a photocatalytic H_2 production performance. In the case of verifying the photocatalytic hydrogen evolution capacity of GDY/g-C_3N_4, they carried out a series of tests, as shown as Fig. 10f–i. The H_2 generation rate of the 0.5% GDY/g-C_3N_4 (0.5 wt% GDY in GDY/g-C_3N_4) was 39.6 μmol h^{-1} under visible light, which was higher than g-C_3N_4 and other GDY/g-C_3N_4 materials. Furthermore, 0.5% GDY/g-C_3N_4 for H_2 evolution reaction also showed high cyclic stability. The g-C_3N_4 and GDY were coupled to form C–N bands, which could promote the separation of photochargic carriers, extend the charge carrier lifetime, enhance the electron density, reduce the reaction overpotential, and promote electron mobility in the photocatalyst.

β-GDY is an important member of the GY family with potential applications, and is rarely reported at present. Li *et al.*[6] prepared β-GDY by a modified Glaser–Hay coupling reaction. After both theoretical calculation and electronic property measurement, β-GDY has the conductivity of 3.47×10^{-6} S m^{-1} and the work function of 5.22 eV. The produced β-GDY was combined with TiO_2 by hydrothermal method to obtain a TiO_2@β-GDY nanocomposite. The photocatalytic performance of such a nanocomposite was tested by photocatalytic degradation of methylene blue (MB) under UV-visible light conditions, as showed in Fig. 10j and k. The TiO_2@β-GDY with

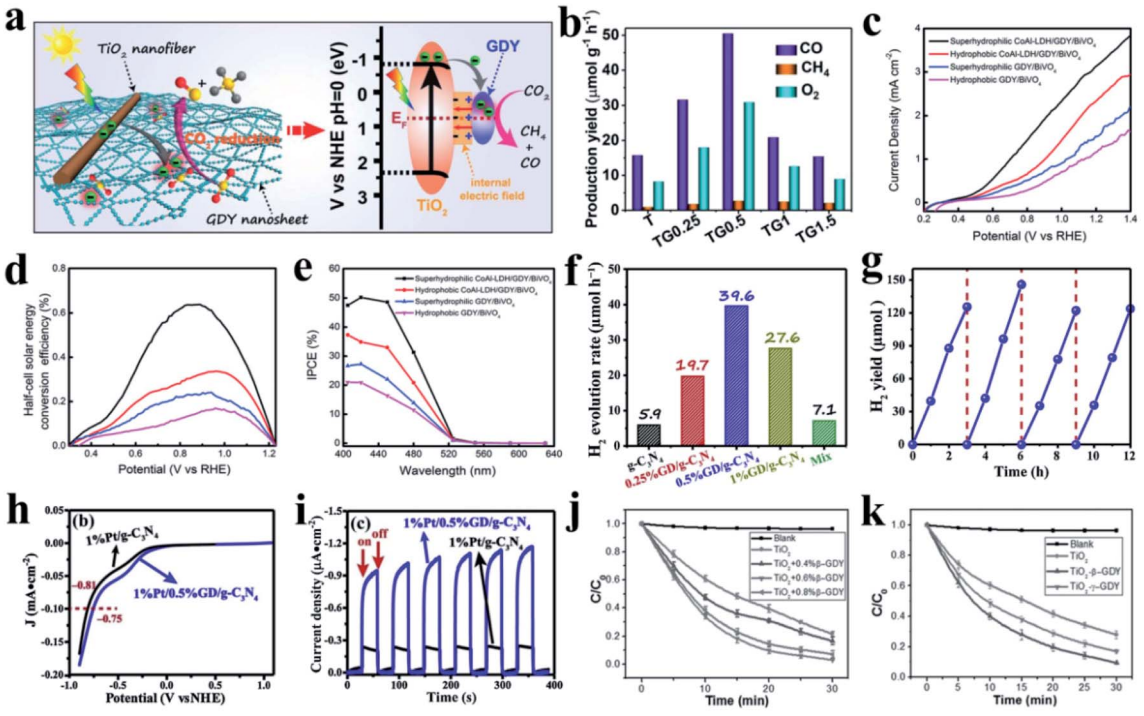

Fig. 10 (a) Schematic illustration of the TiO_2/GDY heterojunction: internal electric field-induced charge transfer and separation under UV-visible light irradiation for CO_2 photoreduction. (b) Photocatalytic activities of CO_2 reduction over the samples. (a and b) Adapted with permission.[113] Copyright 2019, Wiley-VCH. (c) LSV curves and (d) the corresponding half-cell solar energy conversion efficiency for the superhydrophilic GDY/$BiVO_4$, CoAl-LDH/GDY/$BiVO_4$, hydrophobic GDY/$BiVO_4$, and CoAl-LDH/GDY/$BiVO_4$ electrodes under 100 mW cm^{-2} Xe lamp illumination. (e) IPCEs measured at 1.23 V *versus* RHE. (c–e) Adapted with permission.[37] Copyright 2019, Wiley-VCH. (f) Photocatalytic H_2 evolution rate of the prepared samples under visible light (λ > 420 nm). (g) Stability of 0.5% GD/g-C_3N_4 during photocatalytic H_2 evolution. (h) LSV curves. (i) Photocurrent curves. (f–i) Adapted with permission.[114] Copyright 2019, Elsevier B.V. (j) Photocatalytic degradation of MB over TiO_2 and different loading amounts of β-GDY. (k) Photocatalytic degradation of MB over TiO_2, TiO_2@γ-GDY, and TiO_2@β-GDY. (j and k) Adapted with permission.[6] Copyright 2017, Wiley-VCH.

 This journal is © The Royal Society of Chemistry 2020

Published on 30 September 2020. Downloaded by University of Western Ontario on 1/24/2021 7:05:58 PM.

0.6% β-GDY showed a better photocatalytic degradation of MB than other samples with different contents of β-GDY, blank TiO_2 and TiO_2@γ-GDY. This might be owing to the relatively large π-conjugated system in β-GDY, which induced a synergistic effect between TiO_2 and β-GDY for promoting the charge transfer. Compared with γ-GDY, β-GDY could provide more active sites for the Ti atoms, and capture photogenerated electrons from TiO_2. At the same time, β-GDY was also a better electron acceptor with a large number of electron holes, which could effectively inhibit charge recombination and form active groups to promote the degradation of MB.

These results suggested that the addition of GYs into photocatalyst material could improve the electronic density, reduce the electrode overpotential, improve the efficiency of electron hole separation, reduce the charge transfer resistance, and thus enhance photocatalytic performance.

3.2.2 Electrocatalysis. The hydrogen fuel cell is an energy technology with high power density, high energy efficiency and is environmentally-friendly. On the other hand, producing high-purity hydrogen using electrochemical water splitting technology is necessary for sustainable fuel cell technology. Both of these technologies are the research hotspots for energy storage and conversion. At present, high-cost precious metal based electrocatalysts, such as Pt-, Ir-, Ru-based materials, are the practical ones for fuel cells and electrochemical water splitting cells. To reduce the cost, many mainly use precious metal catalysts such as Pt or Pt-based materials, but they are not economical. More nonprecious metals and non-metallic materials have been studied for electrocatalysts, and some promising results have been achieved.[116,117] GDYs and GDYs-based materials have been used in electrocatalysis because of their particular physical and chemical properties. Fig. 11 shows the excellent electrocatalytic activity of GDYs and GDYs-based materials for electrocatalysis. In addition, the GDY-based electrocatalysis has good applications in other fields, such as electrolytic reduction of CO_2 (ref. 12 and 118) and N_2,[119,120] electrocatalytic treatment of organic wastewater,[121] and the electrolytic desulfurization of flue gas and raw coal.[122]

3.2.2.1 Oxygen reduction reaction (ORR). ORR plays a vital role in a series of energy conversion devices, such as metal-air batteries and fuel cells. However, this reaction process involves a multistep proton coupled electron transfer process, which is relatively slow in kinetics. Therefore, it is necessary to select suitable catalysts to improve the reaction rate and efficiency. The precious metals and their alloys are by far the best ORR catalysts, but they are scarce and expensive. Developing inexpensive ORR catalysts for high catalytic activity and stability is a major challenge.

GDY can provide a large surface area and many catalytic active sites by itself, and has a great potential application in ORR. Kang *et al.*[28] used DFT calculations to study the catalytic ORR by nitrogen-doped graphdiyne (NGDY). They found that the high catalytic performance of NGDY was due to the synergistic effect between sp-N and sp^2-N, and the ORR activity of NGDY was comparable to that of the Pt-based catalysts. Si *et al.*[11] introduced the Fe & N co-doped graphdiyne (Fe–N-GDY) as a catalyst for ORR in 0.1 M KOH, and a diagram of the preparation process of Fe–N-GDY is shown in Fig. 11a. N atoms replaced carbon atoms in the carbon structure of GDY, while the Fe atoms are connected to the N-GDY by Fe–C or Fe–N bonds. In ORR, N doping is the most common and effective way to modify GDY.[29] It can be combined with the introduction of Fe for more effective catalytic sites, and can result in high catalytic activity. As shown in Fig. 11b, the obtained limiting current density of Fe–N-GDY with 1.5% Fe is close to the commercial Pt/C. It was believed that the special C–C triple bond in GDY could provide more stable bonding sites for Fe atoms and improve the stability of the catalyst. For achieving more electrocatalytic activity sites, they prepared Co and N co-doped GDY (Co–N-GDY),[19] with an active surface area of 1350 $cm^2\ g^{-1}$ calculated by electrochemical surface area, and the strong interaction between the cobalt atoms and GDY was believed to be beneficial to improving the catalyst's stability. As identified, this Co–N-GDY could serve Co–N-GDY as a bifunctional catalyst for both ORR and hydrogen evolution reactions (HER). Lv *et al.*[123] used a facile cross-coupling reaction to control the bonding configuration of N. They prepared a pyridinic nitrogen-doped GDY (PyN-GDY), in which the pyridinic nitrogen as active sites manifested high performance as oxygen reduction electrocatalysts for Zn–air batteries (Fig. 11e). PyN-GDY was composed of a pyridine ring and acetylenic linkers, in which one carbon atom in each benzene ring of GDY was substituted by pyridinic N. As shown in Fig. 11c, the onset potential (E_{onset}), half-wave potential ($E_{1/2}$) and limited current density (j_L) of PyN-GDY were close to Pt/C. It also exhibited excellent stability, which only had about 7 mV of $E_{1/2}$ shift after 5000 potential cycles (Fig. 11d). Guo *et al.*[126] reported that hydrogen-substituted graphdiyne (HsGDY) supported Cu_3Pd (HsGDY/Cu_3Pd) as a catalyst for ORR showed excellent electrocatalytic activity, which had prominent $E_{1/2}$ of 0.870 V and kinetic current density (at 0.75 V) of 57.7 mA cm^{-2}.

As ORR catalysts, GYs have the planar structure of a large π-conjugated system with uniform large hexagonal pores, which are conducive to gas diffusion. In addition, the large specific area of GYs can increase the number of active sites of ORR. In doped GDYs, the heteroatoms can also affect the electronic configuration of GDYs. They induce charge redistribution to make the carbon atoms around the heteroatoms with more positive charges, which are more conducive to the adsorption of O_2. As a result the doped GDYs have more desirable ORR catalytic activity. The ORR catalytic data for GDYs and GDYs-based materials are shown in Table 2.

3.2.2.2 Oxygen evolution reaction (OER) and hydrogen evolution reaction (HER). To reduce the usage of precious metals in electrochemical water splitting cells, both the OER and HER catalyzed by GDYs and GDYs-doped materials have been explored. Si *et al.*[42] reported a hierarchical GDY@NiFe layered double hydroxide (LDH)/CF as a bifunctional catalyst for the water splitting process. Compared with other reference materials in their experiments, the GDY@NiFe-LDH/CF composites showed the best ORR activity and comparable HER activity to 20% Pt/C/CF. Xing *et al.*[130] explored the 3D porous fluorographdiyne networks on carbon cloth (p-FGDY/CC) as the catalyst for both ORR and OER. This catalyst showed better

Published on 30 September 2020. Downloaded by University of Western Ontario on 1/24/2021 7:05:58 PM.

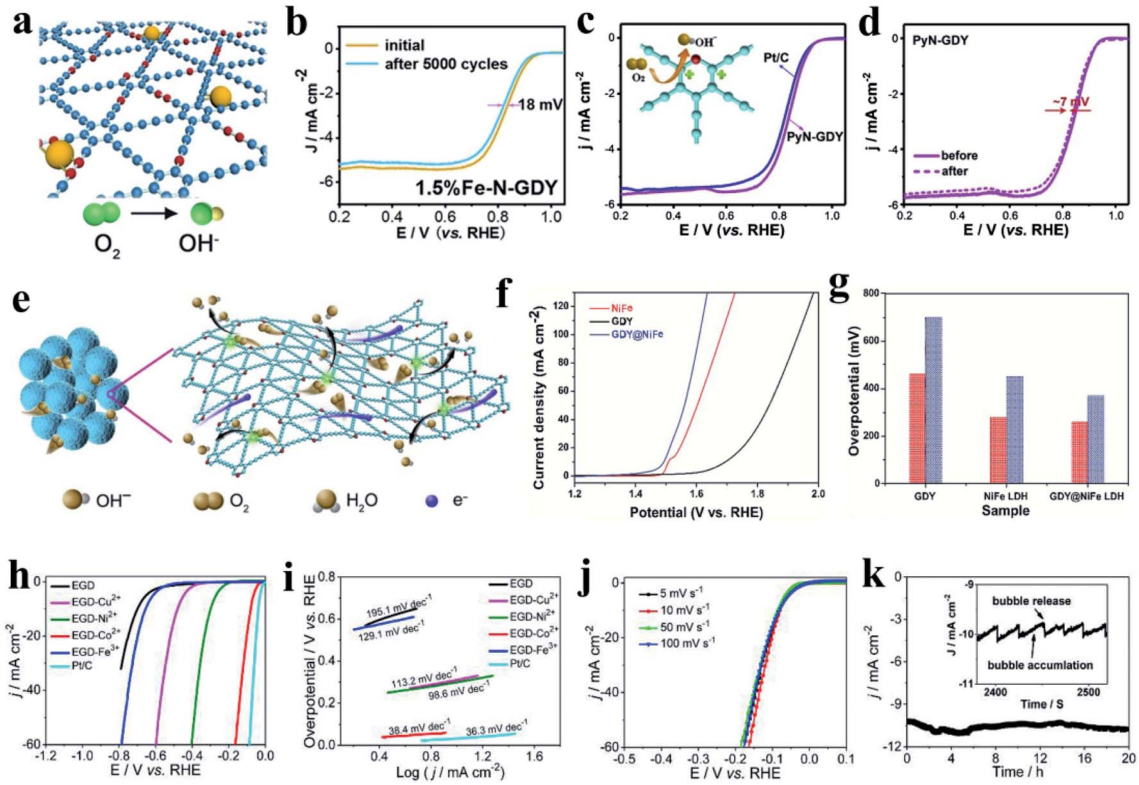

Fig. 11 (a) Schematic diagram for the catalytic process for ORR with 1.5% Fe–N-GDY in 0.1 M KOH. (b) 1.5% Fe–N-GDY at a scan rate of 5 mV s^{-1} before and after 5000 potential cycles in O_2-saturated 0.1 M KOH solution at 1600 rpm. (a and b) Adapted with permission.[11] Copyright 2019, Wiley-VCH. RDE polarization curves of PyN-GDY and Pt/C (JM), (c) and stability curves of PyN-GDY (d) in O_2-saturated 0.1 M KOH solution at a rotating speed of 1600 rpm with a scan rate of 5 mV s^{-1}. (e) Schematic diagram of the process of ORR on PyN-GDY. (c–e) Adapted with permission.[123] Copyright 2020, Elsevier Ltd. (f) Polarization curves for all electrodes with a scan rate of 2 mV s^{-1}. (g) Overpotentials at the current densities of 10 (pink) and 100 mA cm^{-2} (blue) of OER on the GDY@NiFe catalyst. OER performance conducted in 1.0 M KOH solution. (f and g) Adapted with permission.[124] Copyright 2019, American Chemical Society. (h) HER polarization curves and (i) the corresponding Tafel plots for the exfoliated graphdiyne (EGD), EGD-Cu^{2+}, EGD-Ni^{2+}, EGD-Co^{2+}, and EGD-Fe^{3+}, respectively (scan rate: 50 mV s^{-1}). (j) LSV curves of the EGD-Co^{2+} with scan rates from 5 to 100 mV s^{-1}. (k) Time dependence of the current density at −100 mV cm^{-2} (insert shows the enlarged view over 2380–2520 s). (h–k) Adapted with permission.[125] Copyright 2019, Elsevier Ltd.

performance than those reported catalysts for OER in 1.0 M KOH, indicated by their low overpotentials of 82 and 92 mV at the current density of 10 mA cm^{-1} under acidic and alkaline conditions, respectively. This high performance induced by the strong F–C bonding was due to the changed local p–p coupling related electronic orbital fillings. This led to an enhancement of the electron-rich character at the C2 site and higher selectivity for the adsorption/desorption of various O/H intermediate species, resulting in the enhanced ability for electron transfer. Shi *et al.*[124] used GDY-supported NiFe layered double hydroxide (GDY@NiFe) composite *via* electrodeposition method as OER electrocatalyst. Compared with single NiFe and GDY, the

Table 2 GDYs-based materials as catalysts for ORR

Electrocatalysts	E_{onset}, V	$E_{1/2}$, V	j_L, mA cm^{-2}	Tafel slopes (mV dec^{-1})	K–L plots	Ref.
1.5% Fe–N-GDY	0.94	0.82	5.4	89.1	3.87	11
NFLGDY-900c	0.99	0.87	5.2	60	~3.9 at 0.65–0.8 V	82
NFGD	1	0.71	4.5	—	4.2 for 0–0.8 V	127
N0-GDY	0.82	0.69	4.4	—	4	20
N 550-GD/GC	0.95	0.8	4.4	—	3.8	128
N′N-GDY	0.98	0.82	5.1	74	3.84	18
Fe-PANI@GD-900	1.05	0.82	4.4	97.7	4	129
N-HsGDY-900 °C	1.02	0.85	*ca.* 6.2	64.4	3.92	29
N-HsGDY-900 °C	0.86	0.64	4.8	76.7	3.88–3.95 (0.1–0.6 V)	29
1% Co–N-GDY	0.92	0.81	4.01	75	—	19

 This journal is © The Royal Society of Chemistry 2020

Published on 30 September 2020. Downloaded by University of Western Ontario on 1/24/2021 7:05:58 PM.

GDY@NiFe composite had a lower overpotential (Fig. 11f and g). Hu *et al.*[125] reported that doping different non-noble metals could regulate the HER activity of exfoliated graphdiyne (EGD). They found that different non-noble metal atoms had different strength interactions with EGD in the order of $Cu^{2+} < Ni^{2+} < Co^{2+} \ll Fe^{3+}$. The interactions between EGD and M^{n+} ions were very weak and they could be cut off by anionic ions, which had super-strong interaction with metal ions. Then, the M^{n+} ions could bind with these anionic ions and the EGD could be wholly recovered. The M^{n+} ions with EGD that had stronger interaction strength could replace those with weaker interactions. The HER polarization curves and the corresponding Tafel plots of these metal atom-doped EGD in 0.5 M H_2SO_4 are shown in Fig. 11h–k. It was seen that EGD-Co^{2+} gave excellent HER catalytic activity and stability. Wang *et al.*[131] reported that the co-doped few layer GDY of sp-N and S atoms had catalytic OER activity comparable to those of catalysts with single N or S element doped GDY and commercial RuO_2. This was attributed to the fact that the introduction of sp-N and S could significantly reduce the overpotential of the catalyzed electrode, resulting in high catalytic OER current density (Table 3).

3.2.2.3 Other catalytic processes of GYs. Because of the sp- and sp^2-hybridized carbons and the changing of the electron configuration by heteroatom doping, GYs and GYs-based catalysts can also be used in other gas-involved catalytic processes, such as CO_2 evolution reaction (CO_2ER) and nitrogen reduction reaction (NRR). Zhao *et al.*[12] used DFT calculations to investigate the nonmetallic B and N co-doped GDY (B/N-GDY) as electrocatalysts for CO_2ER. The results showed that B/N-GDY had more catalytic active sites and favorable formation energies, which should have high catalytic activity and stability. Du *et al.*[95] used DFT calculations to study the single tungsten atom (W) anchored N-doped GY (W-NGY), and its catalytic performance of nitrogen fixation. A strong interaction between the W atom and N-doped GY was verified by charge transfer. The calculated binding energy of W and N-doped GY through modifying the electron transfer behavior was found to be responsible for the enhanced catalytic activity and stability. The low onset potential of N_2RR was found to be only 0.29 V, indicating this catalyst's high thermodynamic catalytic activity.

The pristine GDY has the semiconducting properties with a band gap of about 0.50 eV.[134] After doping with heteroatoms, the band gap of GDY becomes narrow owing to the spin-up and spin-down bands of the impurity states, and N-doping makes GDY have metal properties. So, N-GDY has both better electrical conductivity and catalytic activity. There is no doubt that GYs and GYs-based materials have great potential in catalysis.

3.3 Applications of GYs as electrode material in energy storage

Lithium/sodium ion batteries (LIBs/SIBs) and supercapacitors have been extensively studied for energy storage devices. They can be used to convert the chemical energy of materials into electrical energy for storage, and then release the electrical energy when used. Carbon materials have widely been used as the electrode materials for many years because of their good electrical conductivity, excellent electron conduction and ion transport ability. GYs as a new type of carbon allotropes are similar to graphene in the aspect of the 2D crystal with a single atomic layer. However, the carbon in GYs is more sp-hybrid than sp^2-hybrid because GYs contain benzene ring structures and alkyne bonds. For example, there are two alkyne bonds between the benzene rings of GDY. The benzene ring and alkyne bond can form a triangular cavity with an area of 6.3 $Å^2$, which is conducive to the diffusion of ions between the GDY layers. Despite its conjugated structure, the GYs were less conductive than graphene because of a certain band gap (0.46–1.22 eV).[65] Since the first synthesis of GDY in 2010, researchers have studied their application in energy storage and conversion in detail through both calculation and experiment. In the following subsections, we will introduce the calculation and application of GYs in LIBs/SIBs and supercapacitors. The summary of the GYs and GYs-based materials as the anode materials of LIBs/SIBs can be shown in Table 4.

3.3.1 Applications of GYs as a new type of carbon anode in LIBs/SIBs. LIBs/SIBs can be electrochemically charged and discharged to store and release electricity energy. In charging/discharging processes, Li^+ and Na^+ are inserted and deinserted between positive and negative electrodes. Thus, the LIBs/SIBs are also vividly called "rocking chair batteries". Due to its large specific surface area, wide layer spacing and excellent

Table 3 GDY and GDY-based materials as catalysts for both OER and HER

Samples	Type (OER or HER)	Electrolyte	Overpotential (mV, 10 mA cm^{-2})	Tafel slopes (mV dec^{-1})	Ref.
GDY@NiFe	OER	1 M KOH	260	95	124
Co-PDY	OER	1 M KOH	270	99	132
NSFLGDY-900	OER	1 M KOH	299	62	131
γ-GDY/Ni foam	HER	1 M KOH	290	59	14
Cu@GD NA/CF	HER	0.5 M H_2SO_4	52	69	92
1% Co–N-GDY	HER	1 M KOH	97	132	19
1% Co–N-GDY	HER	0.5 M H_2SO_4	53	117	19
3D p-FGDY/CC	HER	0.5 M H_2SO_4	92	157	130
p-FGDY/CC	HER	1 M KOH	82	139	130
EGD-Co^{2+}	HER	1 M KOH	−80	38.4	125
GDY/CuS	HER	1 M KOH	106	63.8	133

Published on 30 September 2020. Downloaded by University of Western Ontario on 1/24/2021 7:05:58 PM.

Table 4 Summary of the performance of GYs and GYs-based anodes for LIBs and SIBs

Samples	Devices	Roles	Capacity [mA h g^{-1}]	Current density [mA g^{-1}]	Cycles	Ref.
PY-GDY	LIBs	Anode	1052 (860, 750)	500 (2000, 5000)	100 (400, 1500)	32
PM-GDY	LIBs	Anode	897 (650, 470)	500 (2000, 5000)	100 (400, 4000)	32
HsGDY	LIBs	Anode	1050	100	100	141
Cl-GDY	LIBs	Anode	1150	50	50	81
F-GDY	LIBs	Anode	500	2000	9000	33
P-GDY	LIBs	Anode	1160 (637)	50 (500)	50 (400)	136
S-GDY	LIBs	Anode	380	2000	1000	16
N-GDY	LIBs	Anode	785	200	200	17
TA-GDY	LIBs	Anode	880	2000	500	149
H_1F_1-GDY	LIBs	Anode	2050 (706, 406)	50 (2000, 5000)	50 (3200, 8000)	22
CEY	LIBs	Anode	410	748	120	10
GTY	LIBs	Anode	180	748	200	150
TiO_2-GDY	LIBs	Anode	432.4	1000	300	151
GDY-MoS_2	LIBs	Anode	1450	50	100	152
MnO_2/GDY	LIBs	Anode	660 (450)	200 (1000)	120 (200)	153
γ-GY	LIBs	Anode	948.6 (730.4)	200 (1000)	350 (600)	13
P-TpG	Li-storage	DFT	1979	—	—	154
N-TpG	Li-storage	DFT	2644	—	—	154
C68-GY	Li-storage	DFT	1954	—	—	155
BGDY	SIBs	Anode	600	50	100	156
HsGY	SIBs	Anode	320	5000	5900	38
HsGDY	SIBs	Anode	650	100	100	141
GDY powder	SIBs	Anode	211	100	1000	140
GDY NCs	SIBs	Anode	380	2500	400	40
GDY-NS	SIBs	Anode	405	1000	1000	43
BGY	SIBs	DFT	751	—	—	78

electron transport properties, GDYs have great application potentials in LIBs and SIBs.

As discussed before, in order to enhance the electrochemical property of GDY, many approaches have doped GDY with S,[16] P,[136] F,[33,85] N,[17] and other heteroatoms, which can obtain the modified GDYs with more heteroatom defects and active sites. For example, Huang *et al.*[16] prepared a sulfur-doped GDY (S-GDY) with many C–S–C bonds. The advantage of such materials for negative electrode of batteries is shown in Fig. 12a. As the anode material of LIBs, S-GDY showed better electrochemical properties than pure GDY, such as more stable reversible specific capacity (Fig. 12b and c), which can be attributed to the large number of heteroatom defects and active sites of S-GDY and large specific surface area. When GDYs were doped with P atoms, they exhibited sp^3-orbital configuration and changed the shapes, such as wrinkled surface and distortions, resulting in more active sites. Gao *et al.*[135] reported pyrazinoquinoxaline-based graphdiyne (PQ-GDY) films as anode materials of LIBs and they researched the binding affinities three-stage insertion of 14 lithium atoms by both LIBs measurements and DFT calculations. A lot of pyrazine nitrogens in PQ-GDY can provide more active sites which facilitated the absorption/desorption of Li ions, thus improving the capacity of Li storage. As Fig. 12d showed, PQ-GDY exhibited high capacity and current densities at different current densities. Fig. 12e showed the cycle charge and discharge curves for different cycles, and the corresponding Li adsorption energy E_a by DFT calculations (Fig. 12f). The larger the absolute value of the adsorption energy, it is easier to adsorb Li atoms in the corresponding stage. The Li ions represented by blue balls (at stage a and b) preferentially bound to the pyrazine N atoms. The Li ions represented by yellow balls (at stage c and c) were affected by the lateral butadiyne bond formation regions absorbed on diyne carbon. Finally, the insertion sites of Li ions representedby red balls (at stage c) at central aromatic rings in the PQGDY structure with the lowest E_a. He *et al.*[33] reported on F-doped graphdiyne (F-GDY), which was a fresh 2D carbon framework prepared by the bottom-up strategy. This F-GDY was used as anode materials for LIBs, showing a long cycle life (at a current density of 2000 mA g^{-1}, the reversible capacity of F-GDY was about 490 mA h g^{-1} after 2500 cycles), and the reversible transition from the C–F semi-ionic bond to an ionic bond in the Li storage mechanism by DFT calculations. Kang *et al.*[85] reported that the fluorinated GDY (F-GDY) had a high electrochemical performance for LIBs through enhancing the mechanical properties and conductivity. Compared with the single GDY, F-GDY had a high rate performance and better cycle stability. As Fig. 12g showed, at a current density of 500 mA g^{-1}, the reversible capacity of F-GDY was about 1080 mA h g^{-1} after 600 cycles. Zhang *et al.*[17] studied N-GDY as the anode material for LIBs, which had higher reversible specific capacity and smaller electrolyte resistance. Yang *et al.*[32] also reported the pyrimidine-graphdiyne (PM-GDY) and pyridine-graphdiyne (PY-GDY) films as anode materials for LIBs by qualitatively and quantitatively controlling the nitrogen-doping process. The reversible specific capacities of PY-GDY and PM-GDY were about 764 and 483 mA h g^{-1} after 1500 and 4000 cycles, respectively, at the current density of 5 A g^{-1}. The nanocarbon networks were highly conjugated with pyridinic N heteroatoms and uniform large hexagonal pores. In the meantime,

 This journal is © The Royal Society of Chemistry 2020

Published on 30 September 2020. Downloaded by University of Western Ontario on 1/24/2021 7:05:58 PM.

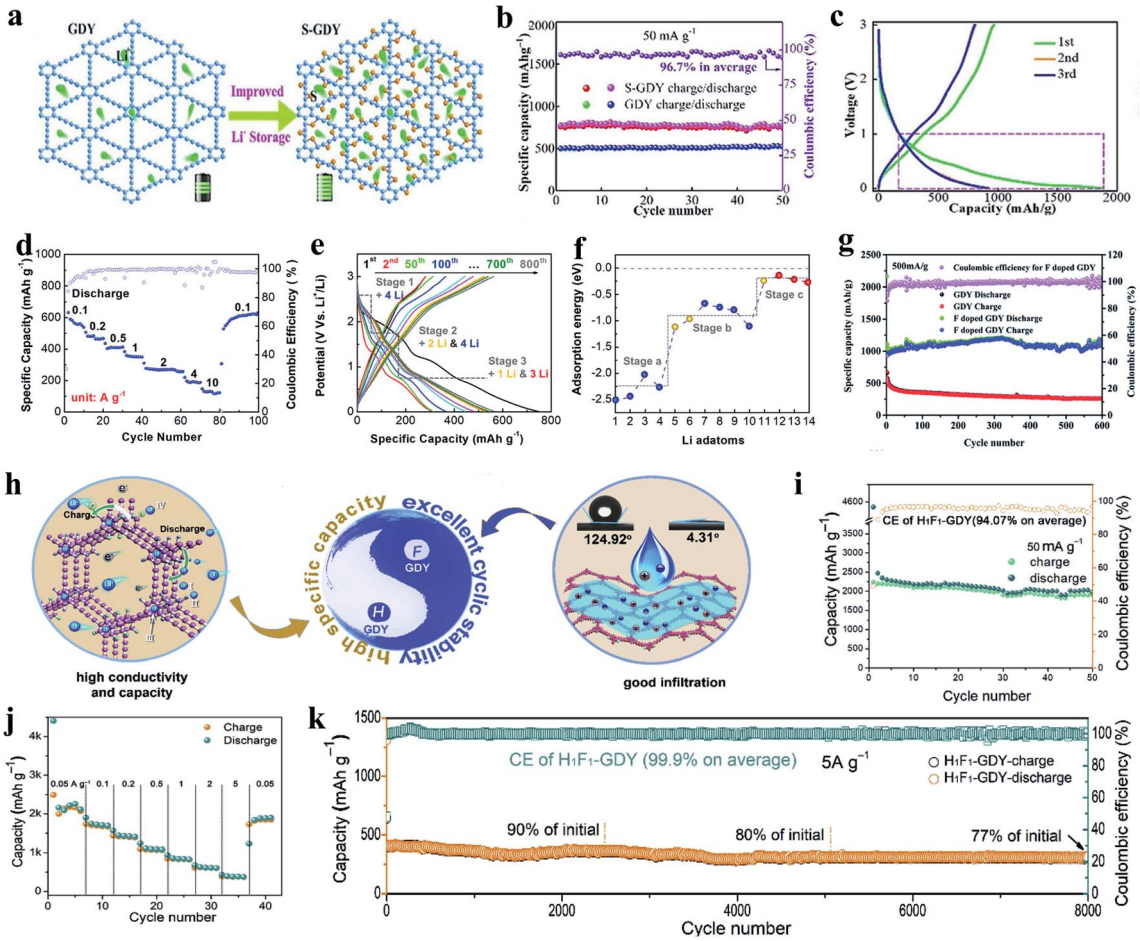

Fig. 12 (a) Illustration of the proposed diffusion of Li ions in GDY and SGDY. (b) Cycle performance of S-GDY- and GDY-based electrodes under 50 mA g^{-1}. (c) Charge–discharge profiles of S-GDY electrodes at 50 mA g^{-1}. (a–c) Adapted with permission.[16] Copyright 2019, Wiley-VCH. (d) Rate performance of the PQ-GDY@Cu electrode; (e) galvanostatic charge/discharge profile of a PQ-GDY@Cu electrode at a current density of 200 mA g^{-1}, recorded between 5 mV and 3 V; (f) adsorption energy as a function of the number of Li adatoms for AB-6 stacking structure. (d–f) Adapted with permission.[135] Copyright 2020, American Chemical Society. (g) Cycle performance of F-GDY and GDY electrodes under 500 mA g^{-1}. Adapted with permission. Copyright 2019, Royal Society of Chemistry. (h) The advantages of H_1F_1-GDY in Li storage. The electrochemical performance of H_1F_1-GDY as an anode for LIBs: (i) rate performance at gradually increasing rates, ranging from 0.05 to 5 A g^{-1}. (j) The cycle performance at 50 mA g^{-1}. (k) The cycle performance of H_1F_1-GDY at 5 A g^{-1}. (h–k) Reproduced with permission.[58] Copyright 2020, Wiley-VCH Verlag GmbH & Co. KGaA, Weinheim.

pyridinic N could enhance the interrelated binding energy, facilitating Li storage.

Due to the synergistic effect between heteroatom and GDY or heteroatoms, the co-doped GDY has a better Li storage capacity than pure GDY or single heteroatom doped GDY. For example, Lu *et al.*[22] used H and F co-doped GDY (H_1F_1-GDY) as the anode materials for LIBs, which showed excellent performance. As shown in Fig. 12h, H-substitution can provide more active sites for lithium intercalation, thus improving the conductivity and capacity of H_1F_1-GDY, and F-substituted can result in the rough surfaces of H_1F_1-GDY. This was beneficial to reducing the surface tension, thus increasing the electrolyte infiltration and facilitating electrolyte diffusion. The H_1F_1-GDY negative electrode was assembled into LIBs for testing the electrochemical properties, and the tested results are shown in Fig. 12i–k. It can be seen that the reversible capacities of H_1F_1-GDY can achieve 2050 mA h g^{-1} at 50 mA g^{-1} after 50 cycles, and retain 406 mA h g^{-1} at 5 A g^{-1} after 8000 cycles. This indicated that the ion transport is fast and stable, and demonstrated the high reversibility of Li storage.

For other types of GYs as anode of LIBs, Cui *et al.*[13] used γ-GY as anode material for LIBs. Due to the 2D mesoporous structure, large conjugate structure, large interplanar distance, and high structural integrity, the electrode of γ-GY showed high electrochemical performances in terms of the reversible specific capacity and cycle stability. At current densities of 200 and 1000 mA g^{-1}, the reversible specific capacities of 948.6 and 730.4 mA h g^{-1} were obtained, respectively. During the processes of charging and discharging, the average coulombic efficiency was maintained at 98%.

As the anode materials for LIBs, GYs-based electrode materials have a large specific surface area, stable structure, highly conjugated nanocarbon networks and well-distributed large hexagonal pores, which can facilitate lithium storage. In particular, in addition to the above points, the doping of the

Published on 30 September 2020. Downloaded by University of Western Ontario on 1/24/2021 7:05:58 PM.

heteroatom-doped GDYs can create more heteroatom defects and electrochemical active sites, thus further improving the electrochemical properties.

SIBs have been extensively explored in recent years because sodium is abundant, inexpensive, and has electrochemical behavior similar to lithium. SIBs have been identified to be promising devices in large-scale energy storage/conversion applications. The GYs as the 2D-layered allotrope of carbon have a large specific surface area, which are a kind of anode materials for SIBs with great potential applications. There are a handful of theoretical and experimental research studies that have been reported on the application of GYs and GYs-based materials in SIBs,[38,43,137–142] and also reviewed in literature.[31,99,143–148] Therefore, in this review, we have summarized some GYs and GYs-based SIBs anode materials in Table 4 for comparison. In general, the GYs are a very promising type of anode material for SIBs. We sincerely hope that by deepening the study and understanding of GYs and GYs-based materials, more advancement can be achieved in the future.

As mentioned above, the GYs-based anode materials for LIBs/SIBs have several advantages. However, in the process of preparing the heteroatom-doped GDYs, the qualitative and quantitative doping of heteroatoms are still a challenge. The application of doped GDYs in energy storage is in its infancy, and there is still a certain gap between the actual capacity of doped GDYs and the theoretical capacity. The above GYs and GYs-based materials have large application potential in LIBs and SIBs devices, which can open up a new research direction of electrode materials for new energy storage devices.

3.3.2 Applications of GYs in supercapacitors. As a new type of energy storage and conversion devices, supercapacitors have the characteristics of quick charge/discharge and high cycle-life, and the energy storage characteristics of the batteries. They store energy through a two-layer interface formed between an electrode and an electrolyte. As a type of carbon materials similar to graphene, GYs are very suitable for negative electrode materials for supercapacitors due to the advantages of the large specific surface area and pore size. However, because the properties of the supercapacitors depend more on the specific surface area of the materials, there are few theoretical calculations of the GYs and GYs-based electrode materials.

Du *et al.*[157] reported the electrochemical properties of the GDY anode and activated carbon (AC) cathode in lithium ion capacitors (LICs). The scheme is shown in Fig. 13a. The GDY exhibited good capacitance behavior at different sweep speeds in the potential range of 2–4 V. At a high sweep rate, the cyclic voltammetric curve was somewhat deformed, mainly due to the partial Faraday reaction (Fig. 13b and c). The galvanostatic charge–discharge (GCD) voltage profiles were triangular, indicating that GDY had an ideal capacitance behavior in the voltage range. Compared with the reported capacitance properties of graphite and graphene, the energy density and power density of GDY were much higher, as indicated by Fig. 13d. The

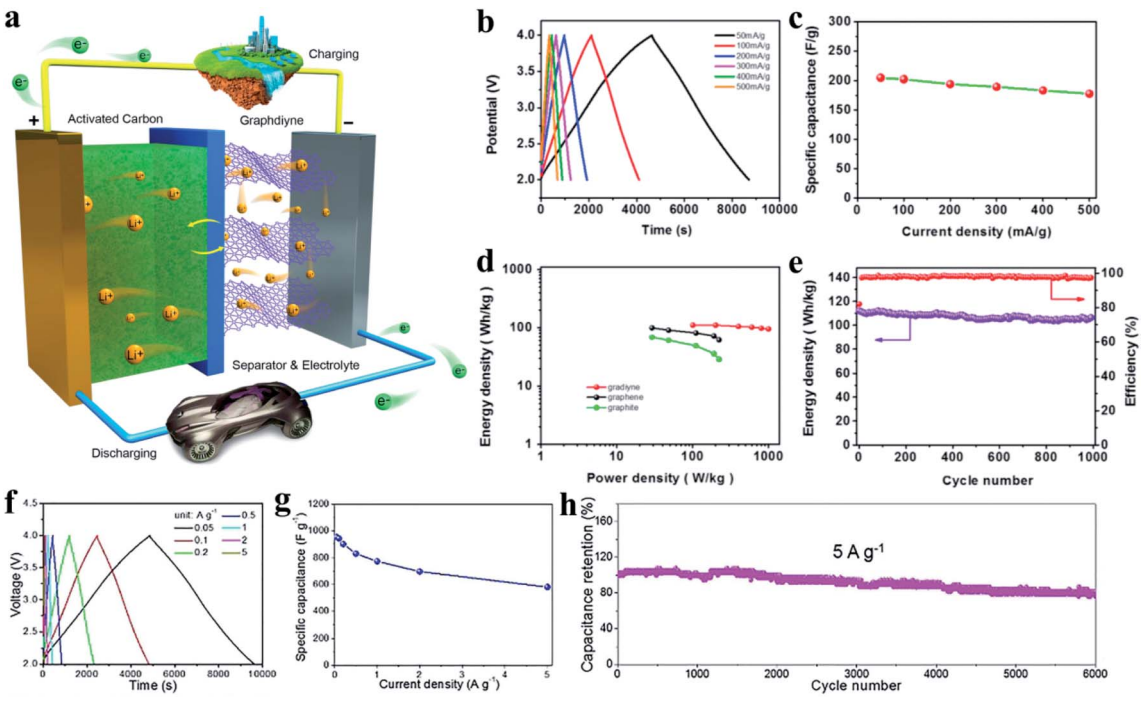

Fig. 13 (a) Scheme of the GDY LICs. Electrochemical characterization of GDY/AC LICs: (b) the GCD voltage profiles at various current densities; (c) the corresponding specific capacitances of the LICs incorporating GDY as the negative electrode at various current densities; (d) Ragone plots of GDY/AC LICs compared with previously reported graphite and grapheme LICs. (e) Cycling stability of GDY/AC LICs at a current density of 200 mA g^{-1}. (a–e) Adapted with permission.[157] Copyright 2016, Elsevier. (f) Galvanostatic charge/discharge profiles at different current densities. (g) Corresponding specific capacitances at different current densities. (h) Cycle stability at a current density of 5 A g^{-1}. (f–h) Adapted with permission.[158] Copyright 2019, Wiley-VCH.

 This journal is © The Royal Society of Chemistry 2020

Published on 30 September 2020. Downloaded by University of Western Ontario on 1/24/2021 7:05:58 PM.

GDY electrode had excellent cycle performance, which was indicated by the energy density of 106.2 W h kg^{-1}, and could be kept to 94.7% after 1000 cycles (Fig. 13e). In this work, they demonstrated that the pore and 2D layered structure of GDY were greatly beneficial to its application in supercapacitors. Shen *et al.*[158] reported on fluorine enriched graphdiyne (F-GDY), which had a 42-C hexagonal porous structure and more evenly distributed fluorine, as well as an excess amount of sp- and sp^2-hybrid carbon atoms. When AC as a cathode and F-GDY (mass ratio of AC *vs.* F-GDY was 7 : 1) as the anode were used in LICs, they showed good reversibly charge–discharge properties (Fig. 13f and g) and excellent long cycle stability with retentions of more than 90% after 3000 cycles and more than 80% after 6000 cycles at 5 A g^{-1}, respectively (Fig. 13h).

Huang *et al.*[159] reported on the N-doped graphdiyne (N-GDY) synthesized through the nitriding of GDY under NH_3 as the negative electrode for LICs and sodium ion capacitors (SICs). The fabrication of this N-GDY/AC LIC (SIC), and the diffusion of Li^+ and Na^+ in N-GDY are shown in Fig. 14a, which indicated the outstanding rate capability, cycle stability, and both high power and energy densities (Fig. 14b and c). At different current densities, the GCD curves showed that the N-GDY/AC LIC had a preferable electrochemical property in comparison to GDY/AC LIC (Fig. 14e). Fig. 14h also showed that N-GDY/AC SIC had higher specific capacitance at various current densities than those of GDY/AC SIC. As shown in Fig. 14f, the maximum energy density of LICs with the N-GDY electrode was 174 W h kg^{-1} at the power density of 112.5 W kg^{-1}, and at a power density of 11 250 W kg^{-1}, the energy density was 107 W h kg^{-1}. The SICs with the N-GDY electrode could keep up an energy density of 119 W h kg^{-1} at a power density of 22 500 W kg^{-1} (Fig. 14i). The energy densities of N-GDY in both LICs and SICs are higher than single GDY and several other carbon materials, which may be due to the greater amount of 3D porous channels, more sites and defects caused by N-doping, and that N-GDY has a better conductivity than other carbon materials.

Heteroatom doping and controllable porosity are important ways to improve the energy storage properties of carbon materials. Yue *et al.*[160] reported a N-doped triazine-based graphdiyne (TGDY), which had a 2D layer-by-layer structure and large specific BET surface area, showed high specific capacitance and long cycle stability. Wang *et al.*[43] explored 3D architecture GDY nanosheets with 3D nanostructure and intramolecular pores as an anode material for SIC (the schematic diagrams of the SICs full-cell configuration is shown in Fig. 15a), which showed both superior energy and power densities together with good cyclic performance and superior reversible specific capacitance (Fig. 15b and c). The SIC delivered a capacitance of more than 200 F g^{-1} over 3000 cycles at a current density of 1 A g^{-1}, and displayed an initial specific energy as high as 182.3 W h kg^{-1} at a power density of 300 W kg^{-1}. In addition, it maintained a specific energy of 166 W h kg^{-1} even at a power density of 15 000 W kg^{-1} (Fig. 15d). Shang *et al.*[20] constructed the well-defined N-doped GDY nanostructure using an explosion

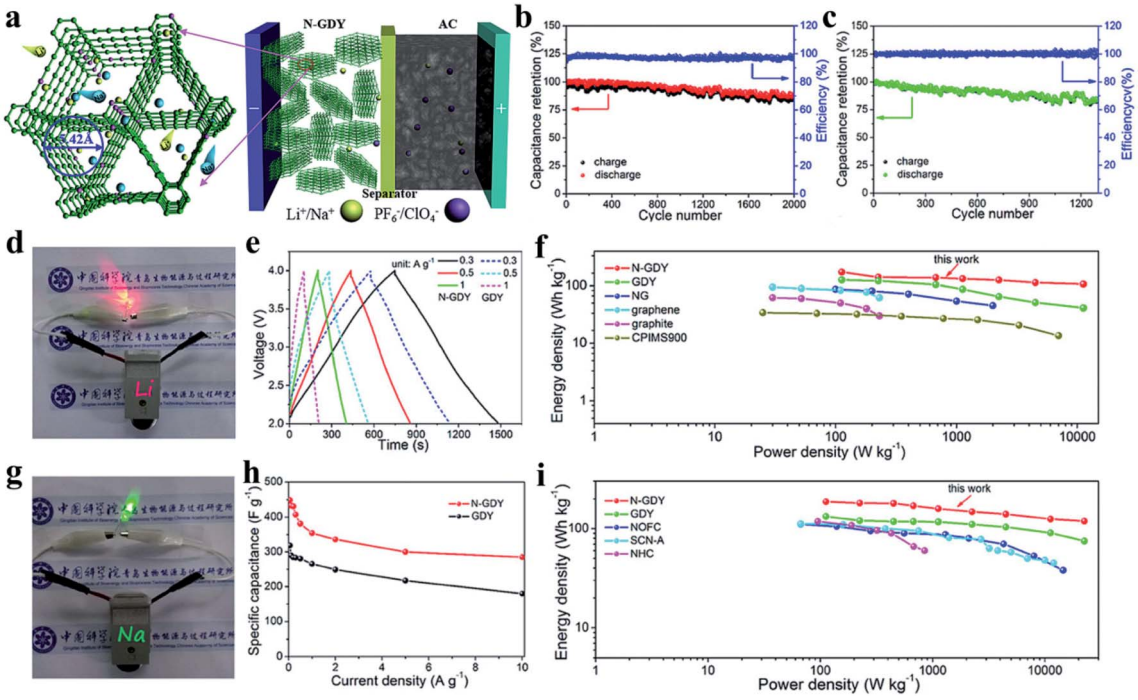

Fig. 14 (a) Schematic illustration of the fabrication of N-GDY/AC LIC (SIC) and diffusion of Li^+ and Na^+ in N-GDY. The cycle stability at 0.2 A g^{-1} of N-GDY/AC LIC (b) and N-GDY/AC SIC (c). (d) Lighting up a light-emitting diode (LED) by N-GDY/AC LIC. (e) GCD curves at the current densities of 0.3, 0.5, and 1.0 A g^{-1}. (f) Ragone plots of N-GDY/AC LIC compared with GDY/AC LIC, previously reported N-rich carbon (NRCS), nitrogen-doped graphene (NG), graphene, graphite LICs. (g) Lighting up a LED by N-GDY/AC SIC. (h) Specific capacitance at different current densities. (i) Ragone plots of the N-GDY/AC SIC compared with GDY/AC SIC, previously reported N and oxygen (O) functionalized carbon (NOFC), KOH activated carbons (SCN-A), and carbon coated-$Na_3V_2(PO_4)_3$ (NHC) SICs. Reproduced with permission.[159] Copyright 2018, Wiley-VCH.

Published on 30 September 2020. Downloaded by University of Western Ontario on 1/24/2021 7:05:58 PM.

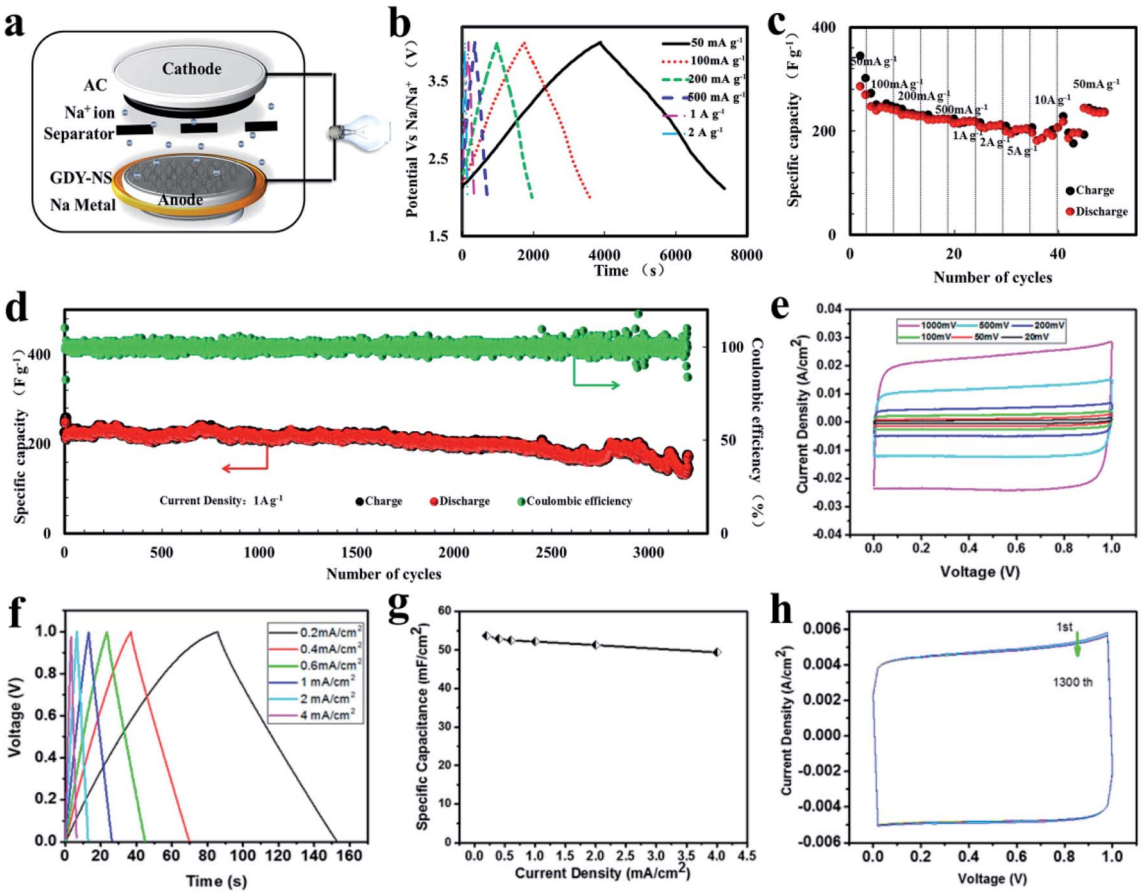

Fig. 15 (a) Schematic diagrams of the SIC full-cell configuration composed of the AC as the cathode and GDY-NS as the anode. (b and c) The GCD voltage profiles of the GDY-NS electrodes at various current densities from 50 mA g^{-1} to 5 A g^{-1}. (d) Cycle performance of the GDY-NS/AC-based SICs at a current density of 1 A g^{-1} (all of the potential *vs.* Na^+/Na). (a–d) Adapted with permission.[43] Copyright 2017, American Chemical Society publications. Supercapacitor performance based on 3D GDY on the nickel foam using a 7 M KOH aqueous electrolyte: (e) CV curves obtained at different scanning rates; (f) galvanostatic charge/discharge profiles under different current densities; (g) specific capacitance retention *via* the current density; and (h) long-term CV at a scanning rate of 200 mV s^{-1} for investigating the cell stability. (e–h) Adapted with permission.[39] Copyright 2019, American Chemical Society publications.

approach. This method could effectively tune the N-configurations (pyridinic N and triazine-like N cluster), N-content, and porous structures of GDYs, showing good controllability with the advantage of application in supercapacitors. The as-prepared GDYs used as the electrode for supercapacitors could provide a specific capacitance of up to 250 F g^{-1}, delivering an energy density of 8.66 W h kg^{-1} and power density of 19.3 kW kg^{-1}. Wang *et al.*[39] explored the 3D GDY nanochains synthesized on arbitrary substrates by an explosion approach as binder-free supercapacitor electrodes, which showed great area capacitance, obvious power properties and excellent long-term retention. As shown in Fig. 15e, the CV profiles under different scan rates were all rectangular in shape, even at a high rate of 1000 mV s^{-1}, meaning a near-ideal capacitance feature. Fig. 15f and g showed the meristic profiles and linear slopes in the galvanostatic charge/discharge curves, further demonstrating that the electrical double layers were effectively formed in the 3D framework. The inconspicuous voltage drop at the top of the meristic triangle revealed low equivalent series resistance. Calculated from the discharge curves in Fig. 15f, the specific area capacitance was 53.66 mF cm^{-2} at a discharge current density of 0.2 mA cm^{-2}. As shown in Fig. 15h, the cell's long-term CV at a scan rate of 200 mV s^{-1} exhibited excellent stability, indicated by the tiny change of the CV curves after 1300 cycles.

The above research studies showed that GYs and GYs-based materials as the negative electrodes of supercapacitors have high power density, energy density and stability. As mentioned above, GYs have large π-conjugated planes, which are conducive to electron migration. Their ordered 3D pore structures, wide layer spacing, and good conductivity due to the existence of C^1 in acetylene bonds are conducive to the rapid adsorption and diffusion of electrons and ions. The unique and stable 3D channel structure formed by multi-layer GYs stacking is also conducive to the reversible adsorption and desorption of small molecules or ions. Because of the existence of these features, GYs and GYs-based materials as the negative materials of supercapacitors can achieve rapid charge and discharge, and then give excellent performance. Therefore, as new carbon negative

 This journal is © The Royal Society of Chemistry 2020

Published on 30 September 2020. Downloaded by University of Western Ontario on 1/24/2021 7:05:58 PM.

electrodes of supercapacitors, GYs and GYs-based materials have significance and application potential in further research studies.

4. Summary, challenges and prospects

4.1 Summary

In this review, we have overviewed the up-to-date achievements in the synthesis of GYs and GYs-based materials as aggregate structures in energy-related applications, including catalysis and energy storage/conversion. As a novel 2D carbon allotrope, GYs have structures of two hybridized forms of sp- and sp^2-carbons. The in-plane pores are circled by the sp- and sp^2-carbons, which drive them to be used in different areas. In catalysis, the positively charged sp-C atoms can adsorb O_2 to drive the ORR process. Moreover, GYs are able to anchor single metal atoms on its surface because of the in-plane pore and acetylenic bonds. They also can be easily doped with other heteroatoms to form active sites for the catalysis applications. In energy storage and conversion, the GYs' in-plane pores supplies not only an abundant number of storage sites for metal atoms, but also transport channels for the smooth diffusion of ions in the direction perpendicular to their plane. The sp^2-carbon atoms maintaining π conjugation can facilitate electron immigration. The excellent performance of GYs and GYs-based materials in these areas suggests that they are the superior alternatives to the other carbon materials.

4.2 Analysis of challenges of GYs

In the past few years, some successes have been achieved by GYs and GYs-based materials. Compared with other carbon-based nanomaterials (such as graphene and carbon nanotubes), GYs are still in their initial exploration stage. The farther applications of GYs still face many challenges and limitations.

4.2.1 First, the fabrication of large-scale single layer GYs remain a challenge. Because of the strong interaction between the GYs layers, the fabricated materials are usually multilayers,[54] which greatly hindered their performance. The preparation process of the GDY precursors is complex and costly, which is one of the most important factors limiting the GDY mass production, modification and extensive research. For γ-GY, it can achieve gram-grade synthesis. The later purification and stripping process is relatively complex, and it is difficult to obtain pure monolayer γ-GY. There are some research studies that have reported on dealing with GYs with few layers, but the processes are time-consuming and complicated (oxidation, multiple centrifugation steps, and dialysis are needed),[161,162] and the yields are not so satisfactory.

4.2.2 Second, some new members are anticipated to be prepared. Most studies on GYs are still in the theoretical stages. GYs with different percentages of acetylenic linkages are anticipated to be prepared in the laboratory, such as 6,6,12-graphyne.[163,164] Unlike γ-graphyne, the 6,6,12-graphyne monolayer (GM) has a unique rhombus acetylene (SA) ring structure and a higher proportion of sp-hybridized carbon atoms. Obviously, the binding interaction of metal to GMs could be further enhanced because of the additional free π electrons in the SA ring. The stability performance of a single atom supported on the 6,6,12-graphyne monolayer could be greatly improved. By theoretical calculation, the possibility of the different configurations of GYs and their potential application value can be predicted, which is of great significance for the targeted synthesis of GYs with different configurations in the lab.

4.2.3 Third, lack of clear understanding of the growth mechanism of GYs. At present, the study of the GDY growth mechanism is still in the stage of theoretical speculation, and there is no experimental data to clearly explain these mechanisms. To make the growth mechanisms for different preparation methods clear, more *operando* techniques are necessary to help understand the mechanism, like *in situ* instrument methods.

4.3 Proposed research directions

The chances always come with the challenges. Because the research studies of GYs are still in their preliminary stage, there are still many research directions we can focus on.

4.3.1 First, further development and optimization of the synthesis strategies to obtain large-scale and high quality GYs. Although GDY could be produced in lab for more than ten years, there is still long way to go for fabrication large-scale and high-quality GYs. To achieve commercialization, simple and large-scale syntheses of the GYs are necessary. Synthesis strategies, like mechanochemical synthesis,[13] are a simple way and easy to scale up. However, the yields need to be further improved, for which the preparation mechanism should be deeply understood.

4.3.2 Second, innate physical and chemical properties of GYs need to be further investigated. The high rate and low coefficients of expansion of GYs-based materials are their superiorities, which have not been sufficiently explored. The full study of these properties may have effective answers for safe batteries without possible explosions or fires caused by the electrode expansion.

4.3.3 Third, building nanostructure compositions with other active materials is considered a very promising research interest for enhancing its performance. With strong demand for high performance of energy storage devices, the desires for electrode materials with higher capacity, excellent rate performance, and long cycle lives are in demand today. In order to meet these requirements, GYs compositing with other active materials may be a way to improve the performance.

All in all, GYs and GYs-based materials emerge as promising materials for applications in many fields, but there are still a number of challenges to overcome. Due to the distinctive performance and characteristics, we think that all of the challenges and limitations will be overcome. GYs will have great potential for future applications.

Conflicts of interest

There are no conflicts to declare.

Published on 30 September 2020. Downloaded by University of Western Ontario on 1/24/2021 7:05:58 PM.

Acknowledgements

This work was financially supported by the National Key Research and Development Program of China (2017YFB0102900).

References

1 G. Yang, L. Li, W. B. Lee and M. C. Ng, *Sci. Technol. Adv. Mater.*, 2018, **19**, 613–648.
2 T. Sattar, *Top. Curr. Chem.*, 2019, **377**, 10.
3 V. B. Mohan, K.-t. Lau, D. Hui and D. Bhattacharyya, *Composites, Part B*, 2018, **142**, 200–220.
4 R. H. Baughman, H. Eckhardt and M. Kertesz, *J. Chem. Phys.*, 1987, **87**, 6687–6699.
5 G. Li, Y. Li, H. Liu, Y. Guo, Y. Li and D. Zhu, *Chem. Commun.*, 2010, **46**, 3256–3258.
6 J. Li, Z. Xie, Y. Xiong, Z. Li, Q. Huang, S. Zhang, J. Zhou, R. Liu, X. Gao, C. Chen, L. Tong, J. Zhang and Z. Liu, *Adv. Mater.*, 2017, **29**, 1700421.
7 Q. Li, Y. Li, Y. Chen, L. Wu, C. Yang and X. Cui, *Carbon*, 2018, **136**, 248–254.
8 B. K. Das, D. Sen and K. K. Chattopadhyay, *Phys. Chem. Chem. Phys.*, 2016, **18**, 2949–2958.
9 D. Malko, C. Neiss, F. Vines and A. Görling, *Phys. Rev. Lett.*, 2012, **108**, 086804.
10 Z. Jia, Z. Zuo, Y. Yi, H. Liu, D. Li, Y. Li and Y. Li, *Nano Energy*, 2017, **33**, 343–349.
11 W. Si, Z. Yang, X. Wang, Q. Lv, F. Zhao, X. Li, J. He, Y. Long, J. Gao and C. Huang, *ChemSusChem*, 2019, **12**, 173–178.
12 J. Zhao, Z. Chen and J. Zhao, *J. Mater. Chem. A*, 2019, **7**, 4026–4035.
13 C. Yang, Y. Li, Y. Chen, Q. Li, L. Wu and X. Cui, *Small*, 2019, **15**, 1804710.
14 Q. Li, C. Yang, L. Wu, H. Wang and X. Cui, *J. Mater. Chem. A*, 2019, **7**, 5981–5990.
15 Y. Lin, H. Liu, C. Yang, X. Wu, C. Du, L. Jiang and Y. Zhong, *Appl. Catal., B*, 2020, **264**, 118479.
16 Z. Yang, W. Cui, K. Wang, Y. Song, F. Zhao, N. Wang, Y. Long, H. Wang and C. Huang, *Chem.–Eur. J.*, 2019, **25**, 5643–5647.
17 S. Zhang, H. Du, J. He, C. Huang, H. Liu, G. Cui and Y. Li, *ACS Appl. Mater. Interfaces*, 2016, **8**, 8467–8473.
18 Q. Lv, W. Si, Z. Yang, N. Wang, Z. Tu, Y. Yi, C. Huang, L. Jiang, M. Zhang, J. He and Y. Long, *ACS Appl. Mater. Interfaces*, 2017, **9**, 29744–29752.
19 X. Wang, Z. Yang, W. Si, X. Shen, X. Li, R. Li, Q. Lv, N. Wang and C. Huang, *Carbon*, 2019, **147**, 9–18.
20 H. Shang, Z. Zuo, H. Zheng, K. Li, Z. Tu, Y. Yi, H. Liu, Y. Li and Y. Li, *Nano Energy*, 2018, **44**, 144–154.
21 W. Zhou, H. Shen, C. Wu, Z. Tu, F. He, Y. Gu, Y. Xue, Y. Zhao, Y. Yi, Y. Li and Y. Li, *J. Am. Chem. Soc.*, 2019, **141**, 48–52.
22 T. Lu, J. He, R. Li, K. Wang and C. Huang, *Energy Storage Materials*, 2020, **29**, 131–139.
23 N. Tian, B.-A. Lu, X.-D. Yang, R. Huang, Y.-X. Jiang, Z.-Y. Zhou and S.-G. Sun, *Electrochem. Energy Rev.*, 2018, **1**, 54–83.
24 J. Lu, Z. Chen, F. Pan, Y. Cui and K. Amine, *Electrochem. Energy Rev.*, 2018, **1**, 35–53.
25 H. Zhang, W. Lu and X. Li, *Electrochem. Energy Rev.*, 2019, **2**, 492–506.
26 M. A. Khan, H. Zhao, W. Zou, Z. Chen, W. Cao, J. Fang, J. Xu, L. Zhang and J. Zhang, *Electrochem. Energy Rev.*, 2018, **1**, 483–530.
27 X. Gao, Y. Dong, S. Li, J. Zhou, L. Wang and B. Wang, *Electrochem. Energy Rev.*, 2019, 1–46.
28 B. Kang, S. Wu, J. Ma, H. Ai and J. Y. Lee, *Nanoscale*, 2019, **11**, 16599–16605.
29 Q. Lv, W. Si, J. He, L. Sun, C. Zhang, N. Wang, Z. Yang, X. Li, X. Wang, W. Deng, Y. Long, C. Huang and Y. Li, *Nat. Commun.*, 2018, **9**, 3376.
30 L. Mengqiu, T. Ling, W. Dong, L. Yuliang and S. Zhigang, *ACS Nano*, 2011, **5**, 2593–2600.
31 N. Wang, J. He, K. Wang, Y. Zhao, T. Jiu, C. Huang and Y. Li, *Adv. Mater.*, 2019, **31**, 1803202.
32 Z. Yang, X. Shen, N. Wang, J. He, X. Li, X. Wang, Z. Hou, K. Wang, J. Gao, T. Jiu and C. Huang, *ACS Appl. Mater. Interfaces*, 2018, **11**, 2608–2617.
33 J. He, N. Wang, Z. Yang, X. Shen, K. Wang, C. Huang, Y. Yi, Z. Tu and Y. Li, *Energy Environ. Sci.*, 2018, **11**, 2893–2903.
34 H. Shang, Z. Zuo, L. Li, F. Wang, H. Liu, Y. Li and Y. Li, *Angew. Chem., Int. Ed.*, 2018, **57**, 774–778.
35 H. Yu, Y. Xue, L. Hui, F. He, C. Zhang, Y. Liu, Y. Fang, C. Xing, Y. Li and H. Liu, *Nano Energy*, 2019, **64**, 103928.
36 X. P. Yin, D. Lu, J. W. Wang and X. L. Lu, *ChemCatChem*, 2019, **11**, 5407–5411.
37 J. Li, X. Gao, Z. Li, J. H. Wang, L. Zhu, C. Yin, Y. Wang, X. B. Li, Z. Liu, J. Zhang, C. H. Tung and L. Z. Wu, *Adv. Funct. Mater.*, 2019, **29**, 1808079.
38 Z. Yang, C. Zhang, Z. Hou, X. Wang, J. He, X. Li, Y. Song, N. Wang, K. Wang and H. Wang, *J. Mater. Chem. A*, 2019, **7**, 11186–11194.
39 F. Wang, Z. Zuo, H. Shang, Y. Zhao and Y. Li, *ACS Appl. Mater. Interfaces*, 2019, **11**, 2599–2607.
40 Z. Zuo, H. Shang, Y. Chen, J. Li, H. Liu, Y. Li and Y. Li, *Chem. Commun.*, 2017, **53**, 8074–8077.
41 R. Liu, X. Gao, J. Zhou, H. Xu, Z. Li, S. Zhang, Z. Xie and a. Z. L. Jin Zhang, *Adv. Mater.*, 2017, **29**, 1604665.
42 H. Si, Q. Deng, L. Chen, L. Wang, X. Liu, W. Wu, Y. Zhang, J. Zhou and H. Zhang, *J. Alloys Compd.*, 2019, **794**, 261–267.
43 K. Wang, N. Wang, J. He, Z. Yang, X. Shen and C. Huang, *ACS Appl. Mater. Interfaces*, 2017, **9**, 40604–40613.
44 K. Wang, N. Wang, J. He, Z. Yang, X. Shen and C. Huang, *Electrochim. Acta*, 2017, **253**, 506–516.
45 J. Zhou, X. Gao, L. Rong, Z. Xie, J. Yang, S. Zhang, G. Zhang, H. Liu, Y. Li, J. Zhang and Z. Liu, *J. Am. Chem. Soc.*, 2015, **137**, 7596–7599.
46 X. Gao, J. Li, R. Du, J. Zhou, M.-Y. Huang, R. Liu, J. Li, Z. Xie, L.-Z. Wu, Z. Liu and J. Zhang, *Adv. Mater.*, 2017, **29**, 1605308.
47 K. Wang, N. Wang, X. Li, J. He, X. Shen, Z. Yang, Q. Lv and C. Huang, *Carbon*, 2019, **142**, 401–410.

 This journal is © The Royal Society of Chemistry 2020

Published on 30 September 2020. Downloaded by University of Western Ontario on 1/24/2021 7:05:58 PM.

48 J. Wang, K. Wang, Z. Yang, X. Li, J. Gao, J. He, N. Wang, H. Wang, Y. Zhang and C. Huang, *ACS Sustainable Chem. Eng.*, 2020, **8**, 1741–1750.
49 J. Li, J. Xu, Z. Xie, X. Gao, J. Zhou, Y. Xiong, C. Chen, J. Zhang and Z. Liu, *Adv. Mater.*, 2018, **30**, 1800548.
50 G. Li, Y. Li, X. Qian, H. Liu, H. Lin, N. Chen and Y. Li, *J. Phys. Chem. C*, 2011, **115**, 2611–2615.
51 S.-S. Wang, H.-B. Liu, X.-N. Kan, L. Wang, Y.-H. Chen, B. Su, Y.-L. Li and L. Jiang, *Small*, 2017, **13**, 1602265.
52 X. Gao, Y. Zhu, D. Yi, J. Zhou, S. Zhang, C. Yin, F. Ding, S. Zhang, X. Yi, J. Wang, L. Tong, Y. Han, Z. Liu and J. Zhang, *Sci. Adv.*, 2018, **4**, eaat6378.
53 L. Wu, Y. Dong, J. Zhao, D. Ma, W. Huang, Y. Zhang, Y. Wang, X. Jiang, Y. Xiang, J. Li, Y. Feng, J. Xu and H. Zhang, *Adv. Mater.*, 2019, **31**, 1807981.
54 R. Matsuoka, R. Sakamoto, K. Hoshiko, S. Sasaki, H. Masunaga, K. Nagashio and H. Nishihara, *J. Am. Chem. Soc.*, 2017, **139**, 3145–3152.
55 X. Qian, Z. Ning, Y. Li, H. Liu, C. Ouyang, Q. Chen and Y. Li, *Dalton Trans.*, 2012, **41**, 730–733.
56 X. Qian, J. Wang, C. Huang, S. Chen, L. Zhang, Y. Li, H. Liu and Y. Li, *Sci. Rep.*, 2015, **5**, 7756.
57 L.-L. Yang, H.-J. Wang, J. Wang, Y. Li, W. Zhang and T.-B. Lu, *J. Mater. Chem. A*, 2019, **7**, 13142–13148.
58 C. Yin, J. Li, T. Li, Y. Yu, Y. Kong, P. Gao, H. Peng, L. Tong and J. Zhang, *Adv. Funct. Mater.*, 2020, 2001396.
59 Z. Zhang, C. Wu, Q. Pan, F. Shao, Q. Sun, S. Chen, Z. Li and Y. Zhao, *Chem. Commun.*, 2020, **56**, 3210–3213.
60 A. M. Morales and C. M. Lieber, *Science*, 1998, **279**, 208–211.
61 X. Duan and C. M. Lieber, *Adv. Mater.*, 2000, **12**, 298–302.
62 Y. Huang, Y. Liang, Y. Rao, D. Zhu, J.-j. Cao, Z. Shen, W. Ho and S. C. Lee, *Environ. Sci. Technol.*, 2017, **51**, 2924–2933.
63 Q. Qu, A. Zhu, X. Shao, G. Shi and Y. Tian, *Chem. Commun.*, 2012, **48**, 5473–5475.
64 Y. Zhang, Y. Xie, T. Ouyang and Y. Chen, *Phys. B*, 2014, **445**, 88–92.
65 X. Zhang, Q. Wang, Z. Jin, Y. Chen, H. Liu, J. Wang, Y. Li and S. F. Liu, *Adv. Mater. Interfaces*, 2018, **5**, 1701117.
66 H. Min, Y. Qi, Y. Chen, Y. Zhang, X. Han, Y. Xu, Y. Liu, J. Hu, H. Liu, Y. Li and G. Nie, *ACS Appl. Mater. Interfaces*, 2019, **11**, 32798–32807.
67 S. Xu, D. Li and P. Wu, *Adv. Funct. Mater.*, 2015, **25**, 1127–1136.
68 M. Liu, Y. Xu, Y. Wang, X. Chen, X. Ji, F. Niu, Z. Song and J. Liu, *Adv. Opt. Mater.*, 2017, **5**, 1600661.
69 H. Liu, J. Guo, M. Guo, F. Wang and Y. Li, *Angew. Chem.*, 2020, DOI: 10.1002/ange.202006891.
70 D. Pan, J. Zhang, Z. Li and M. Wu, *Adv. Mater.*, 2010, **22**, 734–738.
71 Y. Dong, C. Chen, X. Zheng, L. Gao, Z. Cui, H. Yang, C. Guo, Y. Chi and C. M. Li, *J. Mater. Chem.*, 2012, **22**, 8764–8766.
72 J. Lee, K. Kim, W. I. Park, B.-H. Kim, J. H. Park, T.-H. Kim, S. Bong, C.-H. Kim, G. Chae and M. Jun, *Nano Lett.*, 2012, **12**, 6078–6083.
73 J. Lu, P. S. E. Yeo, C. K. Gan, P. Wu and K. P. Loh, *Nat. Nanotechnol.*, 2011, **6**, 247–252.
74 K. Gong, F. Du, Z. Xia, M. Durstock and L. Dai, *Science*, 2009, **323**, 760–764.
75 V. Singh, D. Joung, L. Zhai, S. Das, S. I. Khondaker and S. Seal, *Prog. Mater. Sci.*, 2011, **56**, 1178–1271.
76 I. A. Leonidovich and A. N. Enyashin, *Russ. Chem. Rev.*, 2013, **82**, 735–746.
77 Y. Ma, J. Lin, X.-N. Song, C.-K. Wang, W. Hua and Y. Luo, *Carbon*, 2019, **149**, 672–678.
78 M. Nasrollahpour, M. Vafaee, M. R. Hosseini and H. Iravani, *Phys. Chem. Chem. Phys.*, 2018, **20**, 29889–29895.
79 R. Majidi and A. R. Karami, *Comput. Mater. Sci.*, 2015, **97**, 227–230.
80 B. Mortazavi, M. Shahrokhi, M. E. Madjet, T. Hussain, X. Zhuang and T. Rabczuk, *J. Mater. Chem. C*, 2019, **7**, 3025–3036.
81 N. Wang, J. He, Z. Tu, Z. Yang, F. Zhao, X. Li, C. Huang, K. Wang, T. Jiu, Y. Yi and Y. Li, *Angew. Chem., Int. Ed.*, 2017, **56**, 10740–10745.
82 Y. Zhao, J. Wan, H. Yao, L. Zhang, K. Lin, L. Wang, N. Yang, D. Liu, L. Song, J. Zhu, L. Gu, L. Liu, H. Zhao, Y. Li and D. Wang, *Nat. Chem.*, 2018, **10**, 924–931.
83 W. Xiao, H. Kang, Y. Lin, M. Liang, J. Li, F. Huang, Q. Feng, Y. Zheng and Z. Huang, *RSC Adv.*, 2019, **9**, 18377–18382.
84 Z. Felegari and S. Hamedani, *Results Phys.*, 2017, **7**, 2626–2631.
85 H. Kang, Y. Chen, L. Xu, Y. Lin, Q. Feng, H. Yao and Y. Zheng, *RSC Adv.*, 2019, **9**, 31406–31412.
86 J. Li, S. Li, Q. Liu, C. Yin, L. Tong, C. Chen and J. Zhang, *Small*, 2019, **15**, 1805344.
87 S. Kim, A. Ruiz Puigdollers, P. Gamallo, F. Viñes and J. Y. Lee, *Carbon*, 2017, **120**, 63–70.
88 J. He, S. Y. Ma, P. Zhou, C. X. Zhang, C. He and L. Z. Sun, *J. Phys. Chem. C*, 2012, **116**, 26313–26321.
89 A. Gangan, B. Chakraborty, L. M. Ramaniah and S. Banerjee, *Int. J. Hydrogen Energy*, 2019, **44**, 16735–16744.
90 F. Akbari, A. Reisi-Vanani and M. H. Darvishnejad, *Appl. Surf. Sci.*, 2019, **488**, 600–610.
91 W. Ding, M. Sun, Z. Zhang, X. Lin and B. Gao, *Ultrason. Sonochem.*, 2020, **61**, 104850.
92 Y. Xue, Y. Guo, Y. Yi, Y. Li, H. Liu, D. Li, W. Yang and Y. Li, *Nano Energy*, 2016, **30**, 858–866.
93 W. Zhou, H. Shen, Y. Zeng, Y. Yi and Y. Li, *Angew. Chem.*, 2020, **132**, 4938–4943.
94 J. He, K. Bao, W. Cui, J. Yu, C. Huang, X. Shen, Z. Cui and N. Wang, *Chem.–Eur. J.*, 2018, **24**, 1187–1192.
95 T. He, S. K. Matta and A. Du, *Phys. Chem. Chem. Phys.*, 2019, **21**, 1546–1551.
96 Y. Song, X. Li, Z. Yang, J. Wang, C. Liu, C. Xie, H. Wang and C. Huang, *Chem. Commun.*, 2019, **55**, 6571–6574.
97 S. Z. Butler, S. M. Hollen, L. Cao, Y. Cui, J. A. Gupta, H. R. Gutiérrez, T. F. Heinz, S. S. Hong, J. Huang and A. F. Ismach, *ACS Nano*, 2013, **7**, 2898–2926.
98 S. Guo, Y. Jiang, F. Wu, P. Yu, H. Liu, Y. Li and L. Mao, *ACS Appl. Mater. Interfaces*, 2018, **11**, 2684–2691.
99 J. He, X. Li, T. Lu, X. Shen, N. Wang and C. Huang, *Dalton Trans.*, 2019, **48**, 14566–14574.

Published on 30 September 2020. Downloaded by University of Western Ontario on 1/24/2021 7:05:58 PM.

100 N. Narita, S. Nagai, S. Suzuki and K. Nakao, *Phys. Rev. B: Condens. Matter Mater. Phys.*, 1998, **58**, 11009–11014.
101 Y. Pan, Y. Wang, L. Wang, H. Zhong, R. Quhe, Z. Ni, M. Ye, W. N. Mei, J. Shi and W. Guo, *Nanoscale*, 2015, **7**, 2116–2127.
102 M. Zhang, Y. Li, X. Li, N. Wang and C. Huang, *Adv. Electron. Mater.*, 2020, **6**, 2000157.
103 Y. Li, M. Zhang, X. Hu, X. Fan, L. Yu and C. Huang, *J. Phys. Chem. Lett.*, 2020, **11**, 1998–2005.
104 Y. Pan, Y. Wang, L. Wang, H. Zhong, R. Quhe, Z. Ni, M. Ye, W. N. Mei, J. Shi, W. Guo, J. Yang and J. Lu, *Nanoscale*, 2015, **7**, 2116–2127.
105 M. Jana, R. Xu, X.-B. Cheng, J. S. Yeon, J. M. Park, J.-Q. Huang, Q. Zhang and H. S. Park, *Energy Environ. Sci.*, 2020, **13**, 1049–1075.
106 L. Qiu, Z. He and D. Li, *Adv. Mater.*, 2018, **30**, 1704850.
107 J. Li, L. Zhong, L. Tong, Y. Yu, Q. Liu, S. Zhang, C. Yin, L. Qiao, S. Li, R. Si and J. Zhang, *Adv. Funct. Mater.*, 2019, **29**, 1905423.
108 Y. Ni, L. Miao, J. Wang, J. Liu, M. Yuan and J. Chen, *Phys. Chem. Chem. Phys.*, 2020, **22**, 1181–1186.
109 H. Ren, H. Shao, L. Zhang, D. Guo, Q. Jin, R. Yu, L. Wang, Y. Li, Y. Wang, H. Zhao and D. Wang, *Adv. Energy Mater.*, 2015, **5**, 1500296.
110 H. Shen, Y. Li and Z. Shi, *ACS Appl. Mater. Interfaces*, 2019, **11**, 2563–2570.
111 A. Fujishima and K. Honda, *Nature*, 1972, **238**, 37–38.
112 S. Wang, L. Yi, J. E. Halpert, X. Lai, Y. Liu, H. Cao, R. Yu, D. Wang and Y. Li, *Small*, 2012, **8**, 265–271.
113 F. Xu, K. Meng, B. Zhu, H. Liu, J. Xu and J. Yu, *Adv. Funct. Mater.*, 2019, 1904256.
114 Q. Xu, B. Zhu, B. Cheng, J. Yu, M. Zhou and W. Ho, *Appl. Catal., B*, 2019, **255**, 117770.
115 M. B. Zakaria, C. Li, M. Pramanik, Y. Tsujimoto, M. Hu, V. Malgras, S. Tominaka and Y. Yamauchi, *J. Mater. Chem. A*, 2016, **4**, 9266–9274.
116 Y. He, Q. Tan, L. Lu, J. Sokolowski and G. Wu, *Electrochem. Energy Rev.*, 2019, **2**, 231–251.
117 C. Hu, Y. Xiao, Y. Zou and L. Dai, *Electrochem. Energy Rev.*, 2018, **1**, 84–112.
118 M. Wang, K. Torbensen, D. Salvatore, S. Ren, D. Joulié, F. Dumoulin, D. Mendoza, B. Lassalle-Kaiser, U. Işci and C. P. Berlinguette, *Nat. Commun.*, 2019, **10**, 1–8.
119 L. Hui, Y. Xue, H. Yu, Y. Liu, Y. Fang, C. Xing, B. Huang and Y. Li, *J. Am. Chem. Soc.*, 2019, **141**, 10677–10683.
120 D. Bao, Q. Zhang, F.-L. Meng, H.-X. Zhong, M.-M. Shi, Y. Zhang, J.-M. Yan, Q. Jiang and X.-B. Zhang, *Adv. Mater.*, 2017, **29**, 1604799.
121 Y. Feng, S. Yang, L. Xia, Z. Wang, N. Suo, H. Chen, Y. Long, B. Zhou and Y. Yu, *J. Hazard. Mater.*, 2019, **364**, 562–570.
122 Z. Chen, H. Dong, H. Yu and H. Yu, *Chem. Eng. J.*, 2017, **307**, 553–561.
123 Q. Lv, N. Wang, W. Si, Z. Hou, X. Li, X. Wang, F. Zhao, Z. Yang, Y. Zhang and C. Huang, *Appl. Catal., B*, 2020, **261**, 118234.
124 G. Shi, C. Yu, Z. Fan, J. Li and M. Yuan, *ACS Appl. Mater. Interfaces*, 2019, **11**, 2662–2669.
125 C. Hu, H. Liu, Y. Liu, J.-F. Chen, Y. Li and L. Dai, *Nano Energy*, 2019, **63**, 103874.
126 Y. Guo, J. Liu, Q. Yang, L. Ma, Y. Zhao, Z. Huang, X. Li, B. Dong, X. Z. Fu and C. Zhi, *Small*, 2020, **16**, e1907341.
127 S. Zhang, Y. Cai, H. He, Y. Zhang, R. Liu, H. Cao, M. Wang, J. Liu, G. Zhang, Y. Li, H. Liu and B. Li, *J. Mater. Chem. A*, 2016, **4**, 4738–4744.
128 R. Liu, H. Liu, Y. Li, Y. Yi, X. Shang, S. Zhang, X. Yu, S. Zhang, H. Cao and G. Zhang, *Nanoscale*, 2014, **6**, 11336–11343.
129 Y. Li, C. Guo, J. Li, W. Liao, Z. Li, J. Zhang and C. Chen, *Carbon*, 2017, **119**, 201–210.
130 C. Xing, Y. Xue, B. Huang, H. Yu, L. Hui, Y. Fang, Y. Liu, Y. Zhao, Z. Li and Y. Li, *Angew. Chem., Int. Ed.*, 2019, **58**, 13897–13903.
131 Y. Zhao, N. Yang, H. Yao, D. Liu, L. Song, J. Zhu, S. Li, L. Gu, K. Lin and D. Wang, *J. Am. Chem. Soc.*, 2019, **141**, 7240–7244.
132 H. Huang, F. Li, Y. Zhang and Y. Chen, *J. Mater. Chem. A*, 2019, **7**, 5575–5582.
133 G. Shi, Z. Fan, L. Du, X. Fu, C. Dong, W. Xie, D. Zhao, M. Wang and M. Yuan, *Mater. Chem. Front.*, 2019, **3**, 821–828.
134 J. Koo, M. Park, S. Hwang, B. Huang, B. Jang, Y. Kwon and H. Lee, *Phys. Chem. Chem. Phys.*, 2014, **16**, 8935–8939.
135 L. Gao, X. Ge, Z. Zuo, F. Wang, X. Liu, M. Lv, S. Shi, L. Xu, T. Liu, Q. Zhou, X. Ye and S. Xiao, *Nano Lett.*, 2020, DOI: 10.1021/ acs.nanolett.0c02728.
136 X. Shen, X. Li, F. Zhao, N. Wang, C. Xie, J. He, W. Si, Y. Yi, Z. Yang, X. Li, F. Lu and C. Huang, *2D Mater.*, 2019, **6**, 035020.
137 Z. Xu, X. Lv, J. Li, J. Chen and Q. Liu, *RSC Adv.*, 2016, **6**, 25594–25600.
138 A. H. Farokh Niaei, T. Hussain, M. Hankel and D. J. Searles, *J. Power Sources*, 2017, **343**, 354–363.
139 M. Salavati and T. Rabczuk, *Comput. Mater. Sci.*, 2019, **169**, 109093.
140 S. Zhang, J. He, Z. Jie, C. Huang, Q. Lv, K. Wang, W. Ning and Z. Lan, *J. Mater. Chem. A*, 2016, **5**, 2045–2051.
141 J. He, N. Wang, Z. Cui, H. Du, L. Fu, C. Huang, Z. Yang, X. Shen, Y. Yi and Z. Tu, *Nat. Commun.*, 2017, **8**, 1172.
142 Z. Pan, K. Wang, Y. Wang, P. Tsiakaras and S. Song, *Appl. Catal., B*, 2018, **237**, 392–400.
143 C. Huang, Y. Li, N. Wang, Y. Xue, Z. Zuo, H. Liu and Y. Li, *Chem. Rev.*, 2018, **118**, 7744–7803.
144 A. James, C. John, C. Owais, S. N. Myakala, S. Chandra Shekar, J. R. Choudhuri and R. S. Swathi, *RSC Adv.*, 2018, **8**, 22998–23018.
145 H. Yu, Y. Xue and Y. Li, *Adv. Mater.*, 2019, **31**, e1803101.
146 X. Gao, H. Liu, D. Wang and J. Zhang, *Chem. Soc. Rev.*, 2019, **48**, 908–936.
147 C. Xie, N. Wang, X. Li, G. Xu and C. Huang, *Chem.–Eur. J.*, 2020, **26**, 569–583.
148 R. Sakamoto, N. Fukui, H. Maeda, R. Matsuoka, R. Toyoda and H. Nishihara, *Adv. Mater.*, 2019, **31**, 1804211.

 This journal is © The Royal Society of Chemistry 2020

Published on 30 September 2020. Downloaded by University of Western Ontario on 1/24/2021 7:05:58 PM.

149 Z. Yang, R. Liu, N. Wang, J. He, K. Wang, X. Li, X. Shen, X. Wang, Q. Lv, M. Zhang, J. Luo, T. Jiu, Z. Hou and C. Huang, *Carbon*, 2018, **137**, 442–450.
150 J. Gao, J. Li, Y. Chen, Z. Zuo, Y. Li, H. Liu and Y. Li, *Nano Energy*, 2018, **43**, 192–199.
151 Z. Lin, G. Liu, Y. Zheng, Y. Lin and Z. Huang, *J. Mater. Chem. A*, 2018, **6**, 22655–22661.
152 J. Gao, J. He, N. Wang, X. Li, Z. Yang, K. Wang, Y. Chen, Y. Zhang and C. Huang, *Chem. Eng. J.*, 2019, **373**, 660–667.
153 Y. Lin, H. Kang, M. Liang, X. Ye, J. Li, Q. Feng, Y. Zheng and Z. Huang, *Appl. Surf. Sci.*, 2020, **526**, 146457.
154 B. Mortazavi, M. Shahrokhi, M. E. Madjet, M. Makaremi, S. Ahzi and T. Rabczuk, *Carbon*, 2019, **141**, 291–303.
155 B. Wu, X. Jia, Y. Wang, J. Hu, E. Gao and Z. Liu, *J. Mater. Chem. A*, 2019, **7**, 17357–17365.
156 N. Wang, X. Li, Z. Tu, F. Zhao, J. He, Z. Guan, C. Huang, Y. Yi and Y. Li, *Angew. Chem., Int. Ed.*, 2018, **57**, 3968–3973.
157 H. Du, H. Yang, C. Huang, J. He, H. Liu and Y. Li, *Nano Energy*, 2016, **22**, 615–622.
158 X. Shen, J. He, K. Wang, X. Li, X. Wang, Z. Yang, N. Wang, Y. Zhang and C. Huang, *ChemSusChem*, 2019, **12**, 1342–1348.
159 X. Shen, Z. Yang, K. Wang, N. Wang, J. He, H. Du and C. Huang, *ChemElectroChem*, 2018, **5**, 1435–1443.
160 Y. Yue, Y. Xu, F. Kong, Q. Li and S. Ren, *Carbon*, 2020, **167**, 202–208.
161 L. Zhao, Y. Jiang, J. Hao, H. Wei, W. Zheng and L. Mao, *Sci. China: Chem.*, 2019, **62**, 1414–1420.
162 H. Wang, K. Deng, J. Xiao, C. Li, S. Zhang and X. Li, *Sens. Actuators, B*, 2020, **304**, 127363.
163 M. D. Kilde, A. H. Murray, C. L. Andersen, F. E. Storm, K. Schmidt, A. Kadziola, K. V. Mikkelsen, F. Hampel, O. Hammerich and R. R. Tykwinski, *Nat. Commun.*, 2019, **10**, 1–9.
164 Y. Ni, K.-L. Yao, H.-H. Fu, G.-Y. Gao, S.-C. Zhu, B. Luo, S.-L. Wang and R.-X. Li, *Nanoscale*, 2013, **5**, 4468–4475.